


Spring 1-1-2015

New Spiral Wound Bioelectrochemical Systems and Control Automation for Energy Production and Wastewater Treatment

Alexander John Haeger
University of Colorado at Boulder, ahaeger1@gmail.com

Follow this and additional works at: https://scholar.colorado.edu/cven_gradetds

 Part of the [Civil Engineering Commons](#), [Electro-Mechanical Systems Commons](#), and the [Environmental Engineering Commons](#)

Recommended Citation

Haeger, Alexander John, "New Spiral Wound Bioelectrochemical Systems and Control Automation for Energy Production and Wastewater Treatment" (2015). *Civil Engineering Graduate Theses & Dissertations*. 177.
https://scholar.colorado.edu/cven_gradetds/177

This Thesis is brought to you for free and open access by Civil, Environmental, and Architectural Engineering at CU Scholar. It has been accepted for inclusion in Civil Engineering Graduate Theses & Dissertations by an authorized administrator of CU Scholar. For more information, please contact cuscholaradmin@colorado.edu.

NEW SPIRAL WOUND BIOELECTROCHEMICAL SYSTEMS AND CONTROL
AUTOMATION FOR ENERGY PRODUCTION AND WASTEWATER
TREATMENT

by

Alexander John Haeger

B.S., University of Wisconsin 2012

A thesis submitted to the
Faculty of the Graduate School of the
University of Colorado in partial fulfillment
of the requirement for the degree of
Master's of Science

Department of Civil, Architectural, and Environmental Engineering

2015

This thesis entitled:

NEW SPIRAL WOUND BIOELECTROCHEMICAL SYSTEMS AND CONTROL
AUTOMATION FOR ENERGY PRODUCTION AND WASTEWATER
TREATMENT

written by Alexander John Haeger
has been approved for the department of Civil, Architectural, and Environmental
Engineering

Dr. Zhiyong Ren

Dr. Karl Linden

Dr. JoAnn Silverstein

Date

*The final copy of this thesis has been examined by the signatories, and we
find that both the content and the form meet acceptable presentation standards
of scholarly work in the above mentioned discipline.*

ABSTRACT

Haeger, Alexander John (Master's, Civil, Architectural, and Environmental Engineering)

New Spiral Wound Bioelectrochemical Systems and Control Automation for Energy Production and Wastewater Treatment

Thesis directed by Associate Professor Zhiyong Ren

Wastewater treatment is a hallmark of advanced society and has evolved throughout history to improve treatment efficiency while reducing harmful effects to humans and surrounding ecosystems. The water-energy nexus is no more apparent than in wastewater treatment and much work is being done currently to reduce the energy footprint of the industry. Anaerobic technologies are at the forefront of this energy revolution because they are capable of producing energy products while performing treatment. One such anaerobic technology is the bioelectrochemical system (BES).

Exoelectrogenic bacteria in BESs oxidize organics while producing direct electrical current. While much work has been done in the field, until now, a bottleneck to BES deployment has been the lack of a scalable reactor configuration. In this study a new compact and high performance spiral wound microbial fuel cell (a type of BES) configuration was developed for wastewater treatment. The 3" long configuration

showed high power output of 170 W/m^3 treated (effective reactor volume), low internal resistances of under 1Ω (ohmic), high electrode surface area to volume ratios of $700 \text{ m}^2/\text{m}^3$, and treatment capacity of 9.01 kgCOD/day . An automated electrolyte feeding system was also developed as a part of this study to maintain the highest possible system performance during experiments. Power output and hydraulic dead space both increased with electrode packing density, which is a new insight for the spiral wound design.

The manufacturing methods developed for spiral wound BES modules were successfully applied to microbial capacitive deionization (MCD) for oil and gas produced water treatment. 40" long reactors were built with the aid of a custom machine and maximum power and current outputs of 89 W/m^3 and 228mA were achieved while removing over 68% of the COD in real produced water. The large scale reactor removed 10.2 gTDS/day although external power was required for the integrated desalination process due to a design error. Custom monitoring and control systems were also developed for the MCD system with a focus on operational simplification for field deployment. As a part of ongoing work, material and process improvements can be made to improve the energy efficiency of the desalination system.

DEDICATION

This thesis is dedicated first to my parents Bob and Cindy for their support in all of my endeavors through the years that have led me to where I am today. To my sports coaches Mark and Erik, lab mates Kyle, Casey, and Tyler, and climbing partners Teddy B, Captain K, and Kevin that have not only taught me how to push through the hard times, but have also been there when it was time to turn back and start anew. And finally to all of my family, friends, and loved ones who have shared in the memories of the many adventures that keep me pushing on.

ACKNOWLEDGEMENTS

I must acknowledge my advisor Dr. Zhiyong “Jason” Ren for his guidance throughout the studies presented in this thesis. His honesty and support have been essential in my development as a scientist engineer. I must also acknowledge the National Science Foundation and the Office of Naval Research for their support of my projects through funding.

CONTENTS

Chapter

I.	INTRODUCTION	1
	Motivations for Research Topic	1
	Scope of the Study	4
	Arrangement of the Thesis.....	4
II.	HIGH PERFORMANCE SPIRAL WOUND MICROBIAL FUEL CELL WITH HYDRAULIC CHARACTERIZATION.....	5
III.	OIL AND GAS PRODUCED WATER TREATMENT WITH SPIRAL WOUND MICROBIAL CAPACITIVE DEIONIZATION.....	22
IV.	AUTOMATION OF BIOELECTROCHEMICAL SYSTEMS AND CAPACITIVE DEIONIZATION OR LABORATORY AND FIELD APPLICATION.....	44
V.	CONCLUSION.....	62
	REFERENCES.....	65
APPENDIX		
A.	AUTOMATED CHEMICAL CATHOLYTE FEEDING PROGRAM FOR MICROBIAL FUEL CELLS.....	68
B.	AUTOMATED CONDUCTIVITY AND VOLTAGE MONITORING PROGRAM FOR MCD AND CDI.....	72
C.	SYSTEM STATE CONTROL PROGRAM FOR CDI AND MCD.....	78

TABLES

Table

1. Pilot-scale material dimensions	34
--	----

FIGURES

1. THE (A) IMAGE, (B) SCHEMATIC, AND (C) FLOW DISTRIBUTION OF THE SPIRALLY-WOUND MFC. ANOLYTE FLOWS IN A SPIRAL-FASHION THROUGH THE ANODE PACKET (YELLOW) WHILE CATHOLYTE FLOWS WITHIN THE PVC HOUSING, SATURATING THE CATHODE ELECTRODE (BLACK) BUT NEVER ENTERING THE ANODE PACKET. 9
2. DETAILED FLOW DIAGRAM OF THE SINGLE MANIFOLD SWMFCs, WHICH ALLOW FOR MORE ROBUST SEALS BETWEEN THE CEM (YELLOW) AND RUBBER GASKET (BLUE). THE U-SHAPED ANOLYTE FLOW PATH (RED ARROWS) ALLOWED FOR CENTRALIZED FLOW DISTRIBUTION AND COLLECTION AT THE MANIFOLD (WHITE). 10
3. HYDRAULIC RESIDENCE TIME DISTRIBUTION RESULTS REVEAL FLOW DEAD SPACE WITHIN THE REACTORS. THE Y-AXIS REPRESENTS THE RATIO OF INFLUENT CONCENTRATION TO EFFLUENT CONCENTRATION OF THE STEP INFLUENT TRACER. THE TIME DIFFERENCE BETWEEN THE THEORETICAL (VERTICAL DASHES) AND EXPERIMENTAL (DOTTED LINES) BREAKTHROUGH CURVES IS EVIDENCE OF DEAD SPACE, WHILE THE SKEWNESS OF THE DATA IS EVIDENCE OF DISPERSION WITHIN THE NEAR-PFR REACTORS. 13
4. VOLTAGE PROFILE OF THE TWO CONTINUOUS FLOW SWMFCs. 15
5. POWER OUTPUT: (A) LINEAR SWEEP VOLTAMMETRY RESULTS SHOWING POLARIZATION AND POWER DENSITY CURVES OF TWO DIFFERENT HRTs (20 MIN VS. 40 MIN) AND TWO DIFFERENTLY PACKED SWMFCs (SW-1 VS. SW-2). (B) POWER DENSITY COMPARISON. TOTAL POWER DENSITY IS BASED ON TOTAL ANODIC LIQUID VOLUME, WHILE EFFECTIVE POWER DENSITY IS BASED ON ACTUAL ANODIC FLOW SPACE AS CALCULATED THROUGH HYDRAULIC RTD TESTS. 16
6. NYQUIST PLOTS SHOW LOW OHMIC RESISTANCES IN THE SWMFCs AND RELATIVELY HIGH ACTIVATION AND CHARGE TRANSFER RESISTANCES AT HRTs OF 20 AND 40 MIN (BASED ON TOTAL ANODE VOLUME). 18
7. COD AND COULOMBIC EFFICIENCY: COD REMOVAL RATES (BARS) AND COULOMBIC EFFICIENCIES (LINES) OBTAINED BY THE 2 SWMFCs UNDER DIFFERENT FLOW RATES. SW-2 REMOVED COD AT A FASTER RATE THAN SW-1, WHILE SW-1 ACHIEVED A HIGHER COULOMBIC EFFICIENCY. 19

8. *CDI HAS TWO OPERATIONAL MODES: DESALINATION AND REGENERATION. DURING DESALINATION (A), VOLTAGE IS APPLIED ACROSS A PAIR OF ELECTRODES TO DRAW COUNTERIONS OUT OF SOLUTION. AFTER THE ELECTRODES ARE SATURATED, REGENERATION (B) IS CARRIED OUT BY REMOVING THE POTENTIAL AND IS ACCELERATED BY SHORT-CIRCUITING THE ELECTRODES OR APPLYING REVERSE VOLTAGE.* 25
9. *THE STANDARD CUBOID CONFIGURATION USED IN LAB-SCALE EXPERIMENTS. THIS CONFIGURATION IS IDEAL FOR TESTING ELECTRODES, MEMBRANES, SEPARATORS, AND OTHER SYSTEM VARIABLES, BUT IS NOT FEASIBLE FOR SCALED-UP SYSTEMS.* 27
10. *A CROSS-SECTIONAL VIEW OF THE SWMCD MATERIALS LOADED INTO THE MANIFOLD BEFORE WINDING. ALL MATERIALS BEGIN AS FLAT SHEETS AND ARE WOUND AROUND THE CENTRAL MANIFOLD INTO SPIRAL FORM.* **ERROR! BOOKMARK NOT DEFINED.**
11. *A MACHINE AID WAS BUILT TO HOUSE ALL OF THE SWMCD MATERIALS DURING CONSTRUCTION. WINDING BY HAND PROVED DIFFICULT, SO THE MACHINE WAS USED TO WIND THE MATERIALS AROUND THE MANIFOLDS INTO SPIRAL FORM.....* 29
12. *POOR SEALS FORMED AS A RESULT OF BOTH LOW TENSION DURING MANUFACTURE AND THE USE OF TWO CENTRAL MANIFOLDS. OUTLINED IN RED ARE AREAS WHERE MAJOR GAPS FORMED, WHICH CONCENTRATED NEAR THE MANIFOLDS.....* 30
13. *CONCEPTUAL DRAWING (LEFT) AND FINISHED MACHINE (RIGHT). THE WINCH WAS CONNECTED TO THE AXIS OF ROTATION TO ALLOW INCREMENTAL ROTATION OF THE SPIRAL WHILE MAINTAINING TENSION. TENSION WAS PROVIDED BY THE ROTATIONAL FORCE OF THE WINCH PULLING AGAINST THE COMPRESSION RODS (PARALLEL TO AXIS OF ROTATION).* 31
14. *THE ANODE AND CATHODE CHAMBERS WERE FORMED BY FOLDING A SINGLE SHEET OF IEM AROUND A CENTRAL MANIFOLD. DIMENSIONS SHOWN HERE ARE FOR THE ANODE AND CATHODE. THE BLACK MATERIAL IS ACTIVATED CARBON CLOTH AND THE WHITE AND GREY CHECKERED MATERIAL IS STAINLESS STEEL CURRENT COLLECTOR.* 33
15. *A COMPLETED SWMCD ASSEMBLED WITHIN PVC HOUSING.* 36
16. *THE FULLY ASSEMBLED PILOT MCD SYSTEM.* 36
17. *VOLTAGE PROFILES AS THE ANOLYTE WAS TRANSITIONED TO 100% PRODUCED WATER. OVER THE COURSE OF THREE MONTHS, THE SYSTEM VOLTAGE STABILIZED AROUND 0.6V AS THE MICROBES ACCLIMATED TO THE SALINE ENVIRONMENT AND THE BIOFILM STRENGTHENED.* 38

18. *SALTS (BLUE) AND COD (RED) WERE SUCCESSFULLY REMOVED FROM ALL THREE CHAMBERS OF THE SWMCD. AVOIDING CDI SHORT-CIRCUITING WILL IMPROVE BOTH COD AND TDS REMOVAL IN FUTURE DESIGNS.*..... 41
19. *POWER DENSITY FOR THE PILOT REACTOR OPERATING ON PRODUCED WATER.*..... 42
20. *SCHEMATIC DIAGRAM OF HYDRAULIC FLOWS (SOLID LINES) AND INFORMATION FLOW (DASHED LINES). ANOLYTE (RED) IS RECIRCULATED FROM A 1L HOLDING RESERVOIR. CATHOLYTE (BLUE) IS RECIRCULATED THROUGH THE INTERNAL RESERVOIR WITHIN THE PVC UNTIL REPLACEMENT IS NEEDED. DURING CATHOLYTE DRAINING, VALVE 1 IS OPENED AND CATHOLYTE FLOWS BY GRAVITY INTO AN EFFLUENT RESERVOIR. AFTERWARDS, VALVE 1 CLOSSES AND VALVE 2 OPENS TO FILL THE CATHOLYTE RESERVOIR WITH FRESH SOLUTION. VOLTAGE (DASHED YELLOW) IS READ BY THE ARDUINO MICROCONTROLLER AND THE VALVES (DASHED GREEN) ARE ACTUATED ACCORDINGLY.* 49
21. *AN MFC MUST BE OPERATING OPTIMALLY BEFORE POWER DENSITY TESTS ARE RUN. ANOLYTE AND CATHOLYTE ARE USUALLY REPLACED SIMULTANEOUSLY BEFORE TESTING BEGINS, BUT WITH AUTOMATED CATHOLYTE REPLACEMENT VOLTAGE CAN BE BOOSTED TO HIGH LEVELS. OVER THE COURSE OF ABOUT ONE DAY, VOLTAGE WAS BOOSTED FROM 0.2V TO OVER 0.5V AND MAINTAINED THERE UNTIL POWER DENSITY TESTING. FREQUENT REPLACEMENT OF THE CATHOLYTE ENSURED THE POWER DENSITY RESULTS PRESENTED WERE THE HIGHEST POSSIBLE.* 51
22. *MAINTAINING HIGH PERFORMANCE OVER TIME REQUIRES MAINTAINING ALL ELECTROLYTES AT OPTIMAL CONCENTRATIONS. IN THIS CASE, THE CATHOLYTE WAS THE LIMITING FACTOR. BETWEEN POWER DENSITY TESTING THE AUTOMATED CATHOLYTE REPLACEMENT SYSTEM MAINTAINED SYSTEM PERFORMANCE FOR OVER ALMOST THREE DAYS WITHOUT NEEDING TO REPLENISH THE ANOLYTE.*..... 52
23. *FOLLOWING PUTTING THE AUTOMATION SYSTEM INTO AN IDLE STATE, SYSTEM PERFORMANCE DROPS. THE AUTOMATION SYSTEM CAN BE ADAPTED TO MAINTAIN SUB-OPTIMAL PERFORMANCE IN THE FIELD TO MINIMIZE CATHOLYTE USE WHILE MAINTAINING ADEQUATE COD REMOVAL AND POWER PRODUCTION.* 53
24. *A NOVEL FLOW-THROUGH MCD WAS FOR ABIOTIC TESTING OF THE CDI USING CONTROL AUTOMATION.* 55
25. *PROCESS DIAGRAM FOR THE SEPARATED SYSTEM STATE CONTROLS AND DATA ACQUISITION AND MONITORING SYSTEMS. ONE ARDUINO UNO R3 WAS USED FOR EACH OF THE TWO SYSTEMS, WHICH WERE POWERED SEPARATELY THROUGH 9V 1A AC/DC WALL ADAPTERS.*..... 57
26. *CONTROL WAS CARRIED OUT BY TWO RELAY SWITCHES PER REACTOR THAT WERE CONTROLLED BY A STANDALONE ARUDINO UNO R3.* 58

27. DATA ACQUISITION AND MONITORING WAS CARRIED OUT BY FOUR EC 3.0 CONDUCTIVITY CIRCUITS (ATLAS SCIENTIFIC) CONNECTED TO AN ARDUINO UNO R3. THIS SYSTEM WAS CONNECTED TO A COMPUTER SERIALLY WHERE DATA WAS SENT BY THE ARDUINO TO A MS EXCEL SPREADSHEET.	58
28. A SNAPSHOT OF THE RAW CONDUCTIVITY (YELLOW) AND VOLTAGE (RED) DATA OUTPUT IN MS EXCEL. DURING VOLTAGE APPLICATION, EFFLUENT CONDUCTIVITY DROPS IMMEDIATELY AND EVENTUALLY RISES UP TO THE INFLUENT CONDUCTIVITY. SHORT CIRCUITING TO ZERO VOLTS RELEASES IONS BACK INTO SOLUTION, REGENERATING THE ELECTRODES.	60
29. $C_{IN} - C_{OUT}$ DATA FROM AN EXPERIMENTAL RUN.	61

CHAPTER I

INTRODUCTION

Wastewater treatment has evolved throughout history with a focus on improving treatment efficacy to reduce risk to humans and natural ecosystems. Advanced water treatment is a hallmark of advanced society and access to clean drinking water and adequate wastewater treatment benefits not only the health of humans, but also the health and sustainability of surrounding ecosystems. The United States began investing heavily in municipal sewage treatment in the 1950's with the 1956 Water Pollution Control Act Amendments (WPCAA). Cost-sharing grants were established under the WPCAA and the federal government began paying between 55% and 75% of the cost of sewage treatment projects (USEPA 2001). Construction Grants for sewage treatment facilities in the 1970's and 1980's provided more than \$60 billion and later the Clean Water State Revolving Fund program was put in place to ease the cost burden of construction projects on municipalities (USEPA 2001). Wastewater treatment investment programs have helped the United States become a healthier and more prosperous country, but the vast majority of infrastructure in place is aging and more stringent effluent regulations are imminent. The upgrades needed domestically coupled with wastewater treatment needs in developing countries necessitates rethinking the energy, land, and capital intensive technologies in service presently.

Water and energy are inextricably linked and while research is trending towards highly energy efficient technologies, the most common wastewater treatment systems remain very energy intensive. The activated sludge process was introduced in 1914 and has become the critical process in biological wastewater treatment (Alleman and Prakasam 1983). An active bacterial community is formed when wastewater, usually pre-filtered in settling basins, is aerated to provide adequate electron acceptors for the biological processes. Standard activated sludge is focused on organic removal, but it can be modified to also remove nitrogen and phosphorus if anaerobic selectors are introduced as in the Bardenpho process. To mitigate the high energy cost of activated sludge, sludge post-processing processes such as anaerobic digestion and various value-added biosolids handling techniques have been implemented. Still, despite the high energy content of wastewater, energy recovery processes commonly used are incapable of recovering all of the energy inputs at wastewater treatment facilities. Aeration constitutes 25% of energy use at water and wastewater utilities and likely constitutes a much higher portion at wastewater utilities (USEPA 2008).

In the United States, 0.3 kWh/m³ to 0.6 kWh/m³ (energy input / wastewater volume treated) is required on average for wastewater treatment (McCarty, Bae, and Kim 2011, USEPA 2009). High energy costs represents one of the largest inefficiencies in environmental engineering because the potential energy embodied in the wastewater itself is between 4 and 9 times the energy required for treatment, based on analysis done on real wastewater samples (Shizas and Bagley 2004). Treatment efficacy is paramount, and energy inefficiency improvements are multifaceted and often difficult to design for. When beneficial designs are presented, utilities need to be cautious to protect effluent quality and can be hesitant since most capital improvements require large investments. Despite potential barriers to

change, there is yet a major push in research and development to turn wastewater treatment facilities into energy self-sufficient resource recovery facilities.

Anaerobic wastewater treatment is receiving large amounts of attention as of late for not only energy savings over aeration but also for energy production. Anaerobic digestion (AD) is a well-established technology used to digest wastewater sludge while producing methane. Research on AD is still thriving and many variations of the simple continuous flow stirred tank reactor (CFSTR) design exist. Despite advancements made so far, AD cannot treat raw wastewater efficiently and methane combustion systems are costly. Further, there are risks of releasing methane, which is a very potent greenhouse gas, during AD and methane use. Photobioreactors are also being investigated for algal production of biofuels from wastewater, but no full-scale net energy positive algae systems exist despite years of development. Another anaerobic technology that has been receiving increased attention for its ability to simultaneously treat wastewater and produce electricity in a single step is the bioelectrochemical system (BES).

The BES is a platform technology capable of a variety of wastewater treatment, resource recovery, and energy recovery tasks. In its most basic form, BES contain at minimum two electrodes. Exoelectrogenic bacteria at the anaerobic anode oxidize organics and release electrons to the electrode. Electrons are carried through an external circuit to the cathode where they are used in reduction reactions, usually with oxygen. The electrons produced, potential gradient between electrodes, and other reaction products can be used for desalination, chemical production, hydrogen gas production, and others with added complexity in the configuration of the BES. BES can treat a wide range of organic waste including municipal wastewater, brewery wastewater, dairy farm waste, and oil and gas produced water. Because BES convert waste to electricity in a single step, energy conversion machinery is not

needed, which greatly reduces the capital investment for BESs. The technology has advanced greatly in the past decades, and many research groups are working to balance organic to electricity conversion ratios with practical system configurations. High electrode surface-area to reactor volume ratios are needed to maintain high power densities, but hydraulic dead space and clogging can occur when too much electrode is packed into a reactor. Also, the internal resistance due to charge transfer, ion transfer, and others should be minimized to increase power, but other losses from oxygen diffusion to the anode and manufacturability issues have arisen in past configurations when electrodes have been brought close to one another to achieve this.

In this thesis a new spiral-wound configuration was developed and studied for small and large scale BES reactors first for wastewater treatment and later for coupled wastewater treatment and desalination of oil and gas produced water. Methods to seal the BES materials into spiral-wound modules were first developed for the small spiral study in chapter 2, and later re-evaluated for large and more complex desalination BESs in chapter 3. Preliminary results are presented therein as the scale-up phase of the project is ongoing. Finally, chapter four presents new control systems to automate both basic and more complex BESs while extracting useful data.

CHAPTER II

HIGH PERFORMANCE SPIRAL-WOUND MICROBIAL FUEL CELL WITH HYDRAULIC CHARACTERIZATION

Introduction

The microbial fuel cell (MFC) is a type of bioelectrochemical system that employs exoelectrogenic bacteria to oxidize biodegradable materials and generate electricity (Logan and Rabaey 2012, Wang and Ren 2013, Li, Yu, and He 2014). An MFC generally consists of an anode and a cathode, which are either separated by a porous separator in multi-chambered designs (Zhang et al. 2011, Huggins et al. 2014), or they can be housed in a single chamber without separators (Liu and Logan 2004). Dramatic improvements have been made during the past decade to address the physical and chemical constraints of the technology. Many materials, configurations, and feedstocks have been studied, and standard tests and metrics have been developed to compare and improve system performance while reducing their cost (Logan 2012).

Many research groups are working on scaling up MFCs, and the main configurations being considered include tubular designs, stacked plates, and separator electrode assembly (SEA) (Fan, Han, and Liu 2012, Rabaey et al. 2005, Aelterman et al. 2006, Zhang et al. 2009). However, many challenges remain to be addressed. For example, tubular designs that use ion exchange membranes as both structural support and separators have been operated at liter scales, but water leakage has been reported as a major problem due to high static pressure and

This research was published in *Bioresource Technology* by the author.

Haeger, A., C. Forrestal, P. Xu, and Z. J. Ren. 2014. "High performance spiral wound microbial fuel cell with hydraulic characterization." *Biores. Technol.* no. 174:287-293.

membrane swelling (Aelterman et al. 2006, Jacobson, Drew, and He 2011). Tubular designs use brush anodes surrounded by a layer of cloth cathode, and the resulting cathode surface area is orders of magnitude lower than the brush anode, making it a bottleneck for future improvement. Frame-and-plate stack designs reduce water pressure by dividing the reactor into multiple chambers, and high surface area to volume (S:V) ratios up to $650 \text{ m}^2/\text{m}^3$ have been achieved using thin chambers (Fan, Han, and Liu 2012). The stack is generally rectangular in shape and consists of separated parts including many layers of electrodes, separators, and gaskets. The metal or plastic frames are responsible for sealing the chambers from each other, but providing sufficient and balanced force along all four edges to maintain the seals is problematic at larger scales. SEAs have been assembled in frame-and-plate stacks with low internal resistance by using a cloth separator in a single chamber air-cathode configuration in each cell. Biofilm fouling and low cathode performance are major challenges for SEAs (Fan, Han, and Liu 2012).

Spiral-wound configurations has been widely applied in water purification and desalination processes such as reverse osmosis (RO), pressure retarded osmosis (PRO) and forward osmosis (FO) (Riley et al. 1977, Xu et al. 2010). Such geometry has been shown successful in plug flow type operations due to its larger surface area, compact design, and high throughput. The plug flow reactor (PFR) behavior creates internal concentration polarization along the flow path, which was reported to allow for high substrate removal rates in wastewater treatment (Xu et al. 2010, Benjamin and Lawler 2013). The spiral-wound configuration is promising for BES scale up because they are theoretically capable of achieving PFR-like behavior, can be easily supported structurally, and can achieve high S:V ratios along with high power density compared to similar configurations. Instead of having the electrolytes flow through framed chambers, the electrodes, membrane sheets, and current collectors are

manufactured together into modules, and multiple modules are rolled up around a central manifold in a spiral fashion. Solid tubular housing provides the reactor with equally distributed structural support around all seal areas to reduce the propensity for membrane deformation and localized pressure buildups to cause seal failures. Spiral-wound BES (swBES) are difficult to construct, and so far only one feasibility study reported a power output of 77 W/m³ by using a two chamber design and Pt-catalyst cathode, which was among the highest volumetric power output from two-chamber systems (Jia et al. 2013).

Given the great potential spiral wound configuration brings to BES development, this study reports a new catalyst-free spiral-wound MFC system that demonstrated high S:V ratio and high power output. Two reactors with different electrode packing densities were analyzed using both hydraulic and electrochemical characterization tools, which provided new information on the effects of electrode packing and spacing on power production and hydraulic behavior. Because so far most BES studies have been on fed-batch mode, hydraulic residence time distribution (RTD) studies are not common in BES research. Such studies can provide crucial information on flow patterns and short circuiting, which are very important parameters as scaled-up BESs are becoming increasingly thin and complex. The dead space (percentage of reactor volume that is absent of flow) reveals reactor behavior more like plug-flow, which informs substrate removal and power output predictions (Do-Quang et al. 1999).

Materials and Methods

Reactor Design and Operation

Fig. 1 shows schematic diagrams and an image of the two-chamber swMFC design. In constructing these systems, materials are formed into two modules, the

anode (yellow) and cathode (black), which are wound around a central flow manifold. The anode module is formed into a sealed “packet” with cation exchange membrane (CEM, Membranes International Inc.) forming the outer walls and activated carbon cloth anode (ACC, Chemviron Carbon, UK) and stainless steel current collector contained within. The catalyst-free ACC cathode was placed outside of and directly next to the anode packet so that after winding the materials into a spiral, cathode electrode surrounded the anode chamber on two sides. The anode module was hydraulically and physically connected to the central manifold, as shown in fig. 2, while the cathode module was not. After construction, the spirals were placed within a solid PVC tube of the same diameter that served as the catholyte reservoir along with structural support. Anolyte entered the anode packet through the manifold and flowed along the spiral direction, while catholyte flowed outside of the anode packet, saturating the cathode electrodes within the PVC housing. The single-manifold design yielded a near circular final product that allowed for the strongest seals as well as a tight fit into structurally supporting PVC tubes.

Two swMFCs of the same size (7.6 cm length x 5.1 cm diameter) were built in this study. SW-1 contained one layer of ACC electrode in both the anode and cathode chambers, while SW-2 contained two layers of ACC in each chamber. The anode electrodes and current collectors were measured 6.4 cm x 19.1 cm with a 1.3 cm x 17.1 cm rectangle cut out beginning at one side, and the cathode electrode units were 7.6 cm x 20.3 cm. The swMFCs were inoculated with the same effluent from a functioning MFC and operated identically for all experiments. Since the focus of this paper is on the development of a new MFC configuration and characterization methods, classical 20 mM acetate with 50 mM PBS buffer solution was used for the anolyte solution, and the detailed media information is described in Forrestal et. al 2012 (Forrestal, Xu, and Ren 2012). The catholyte solution contained 1 g/L sodium percarbonate

(oxygen releasing compound) with 50mM PBS (Forrestal et al. 2014). For each swMFC, anolyte was continuously flowed through the anode packets from a feeding reservoir to an effluent reservoir without recirculation, while the catholyte was recirculated continuously through a separate reservoir at a rate of 80 mL/min.

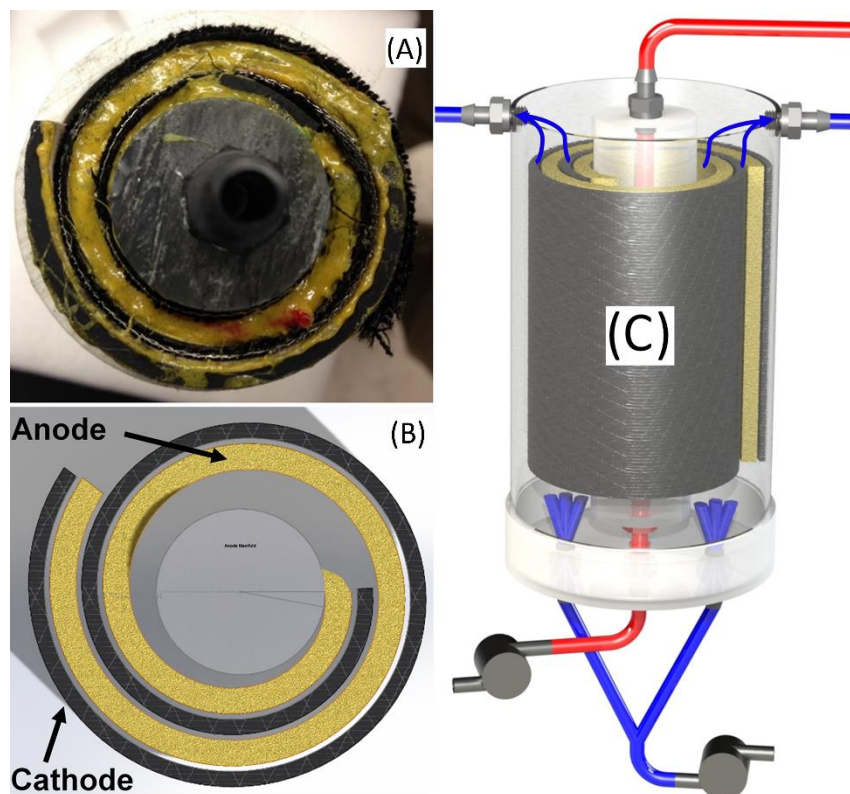


Figure 1: The (A) image, (B) schematic, and (C) flow distribution of the spirally-wound MFC. Anolyte flows in a spiral-fashion through the anode packet (yellow) while catholyte flows within the PVC housing, saturating the cathode electrode (black) but never entering the anode packet.

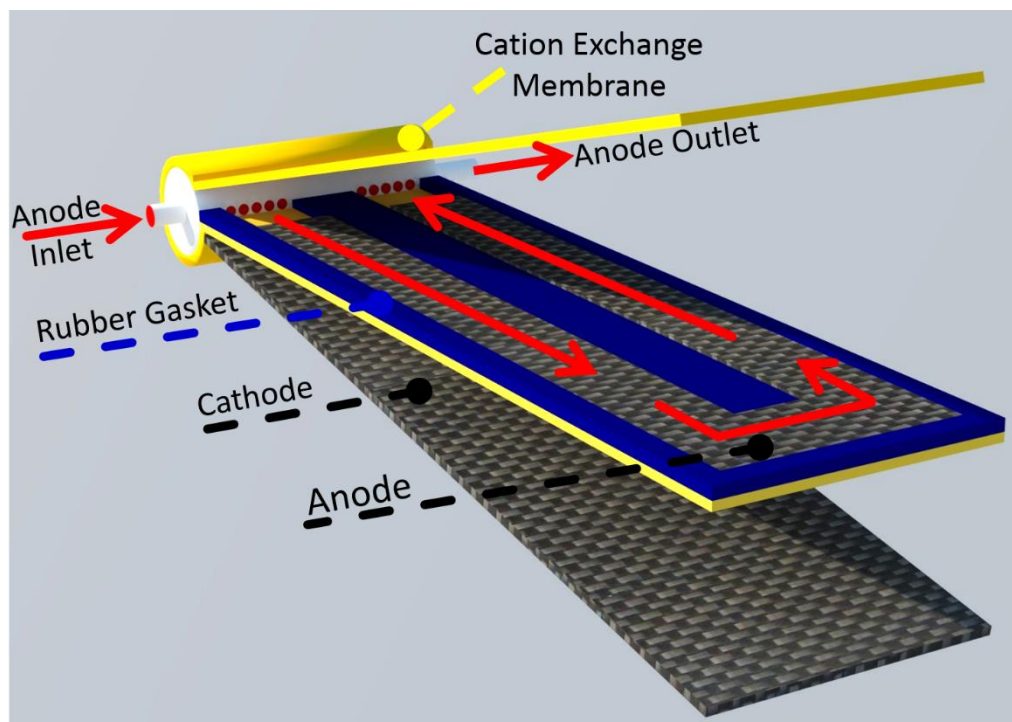


Figure 2: Detailed flow diagram of the single manifold swMFCs, which allow for more robust seals between the CEM (yellow) and rubber gasket (blue). The u-shaped anolyte flow path (red arrows) allowed for centralized flow distribution and collection at the manifold (white).

Hydraulic Residence Time Distribution

Hydraulic residence time distribution (RTD) tests characterize the flow condition and identify hydraulic dead space to inform system efficiency. A step-input tracer study was conducted on the swMFC anodes to study their complex hydraulic patterns by feeding the anode packets with 4 g/L NaCl solution from a continuously mixed beaker. Conductivity at the outlet was measured every 30 seconds until the effluent conductivity matched the influent conductivity. The data collected during RTD tests were analyzed according to accepted principles as outlined below.

The principal result is the cumulative age distribution, which is defined as $F(t) = c_s(t)/c_{in}$, where c_{in} is the influent concentration and $c_s(t)$ is the effluent response concentration at time t . Mean residence time \bar{t} is the statistical average time parcels

of water are likely to stay within the reactor and it can be approximated from the discrete data set of $F(t)$ according to the following equation:

$$\bar{t} \approx \sum_{all\ i} [t_{i,ave} F_i(t)] \quad (1)$$

Effective volume was calculated by dividing \bar{t} by flow rate and dead space was calculated as the difference between theoretical volume, V_{theor} , which is the total anode volume, and V_{eff} .

The spread of the RTD data around \bar{t} can be calculated with statistical variance, $\sigma_{RTD,exp't}^2$, which was found using the equation for reactors with well-defined inlets and outlets (i.e. closed boundaries) as follows:

$$\sigma_{RTD,exp't,closed\ boundaries}^2 = \frac{\sum_{all\ i} [t_{i,ave}^2 c_{i,ave} \Delta t_i]}{\sum_{all\ i} [c_{i,ave} \Delta t_i]} \quad (2)$$

Since the swMFC anode chambers are long and thin packets designed to act similar to plug flow, a plug flow reactor (PFR) model was used to determine how close anode chambers performed to the ideal PFR case. The dispersion number, N_D , which is the ratio of dispersion to advection, was used to match the normalized experimental RTD variance to the model variance. That is to say that,

$$\tilde{\sigma}_{RTD,exp't}^2 = \tilde{\sigma}_{RTD,model, PFR+dispersion, closed\ boundaries}^2 \quad (3)$$

Where,

$$\tilde{\sigma}_{RTD,exp't}^2 = \frac{\sigma_{RTD}^2}{\bar{t}^2} \quad (4)$$

And finally,

$$\tilde{\sigma}_{RTD,model, PFR+dispersion, closed\ boundaries}^2 = 2N_D - 2(N_D)^2 \left\{ 1 - \exp\left(-\frac{1}{N_D}\right) \right\} \quad (5)$$

In equation 3, the left-hand side of the equation can be calculated from the experimental data, while N_D is chosen to satisfy the equality. The resulting N_D is used to determine whether advection or dispersion dominates in the reactor and thus which ideal case the reactors are more similar to. Equations 1-5, background information on RTD analysis and the principles of step-input tracer tests were taken from Benjamin and Lawler, 2013.

Electrochemical and Chemical Characterization

Electrochemical impedance spectroscopy (EIS) and linear sweep voltammetry (LSV) analyses were performed during the study using a Potentiostat (PC4/300, Gamry Instruments, NJ) (Luo et al., 2013). EIS was performed using a 10^5 to 0.01 Hz frequency range and 10mV amplitude (Lu et al. 2014) and LSV was performed with a 1 mV/s scan rate. The compact design did not allow for a reference electrode, so all electrochemistry tests were done in two-electrode mode with the anode as working electrode. Voltage was monitored continuously using a digital data acquisition system (Keithley Instruments Inc., Model 2700). Power output was calculated based on V_{eff} and V_{theor} to represent power density based on effective (P_{eff}) and theoretical, or total, (P_{theor}) anode volume, respectively. COD removal tests were conducted during stable operation 5 days after electrochemical testing under three flow rates (0.2, 0.7, and 1.4 mL/min) while the reactors were connected to 400 Ω external resistances and three effluent samples were taken at 30 minute intervals for each flow rate. Coulombic efficiency was calculated according to the method described before (Logan et al. 2006).

Results and Discussion

RTD Analysis

Fig. 3 shows the results of RTD analysis that reveals flow dead space within the reactors. The experimental cumulative age distribution curve, $F(t)$, represents the ratio of effluent to influent concentration over time, t . The vertical dashed lines represent the expected behavior if the anodes acted as ideal PFRs since the tracer breakthrough would happen instantaneously at the time equal to τ . The time difference between the theoretical (vertical dashes) and experimental (dotted lines) breakthrough curves is indicative of dead space. SW-1 and SW-2 represented different levels of anode packing, with SW-1 containing one sheet of ACC that did not

completely fill the anode volume and SW-2 containing two sheets, which completely filled the anode volume.

The RTD results confirmed the hypothesis that the thin but long anode chambers behaved closely to PFRs and identified improvement potentials in packing thin chambers with appropriate amounts of electrode. Based on the calculation of mean residence time, the dead space ratio of SW-1 was 20%, much smaller than SW-2, which had 67% dead space. While SW-1 and SW-2 had similar total anode volumes of 30 mL and 28 mL respectively, the effective volume of the reactors drastically different at 24 mL and 9.5 mL respectively. The $F(t)$ curves for both reactors are slightly slanted, indicating an amount of mixing (dispersion) along the direction of analyte flow. Dispersion numbers of 0.34 and 0.33 were calculated for SW-1 and SW-2, respectively, confirming that dispersion was present but did not play a large role.

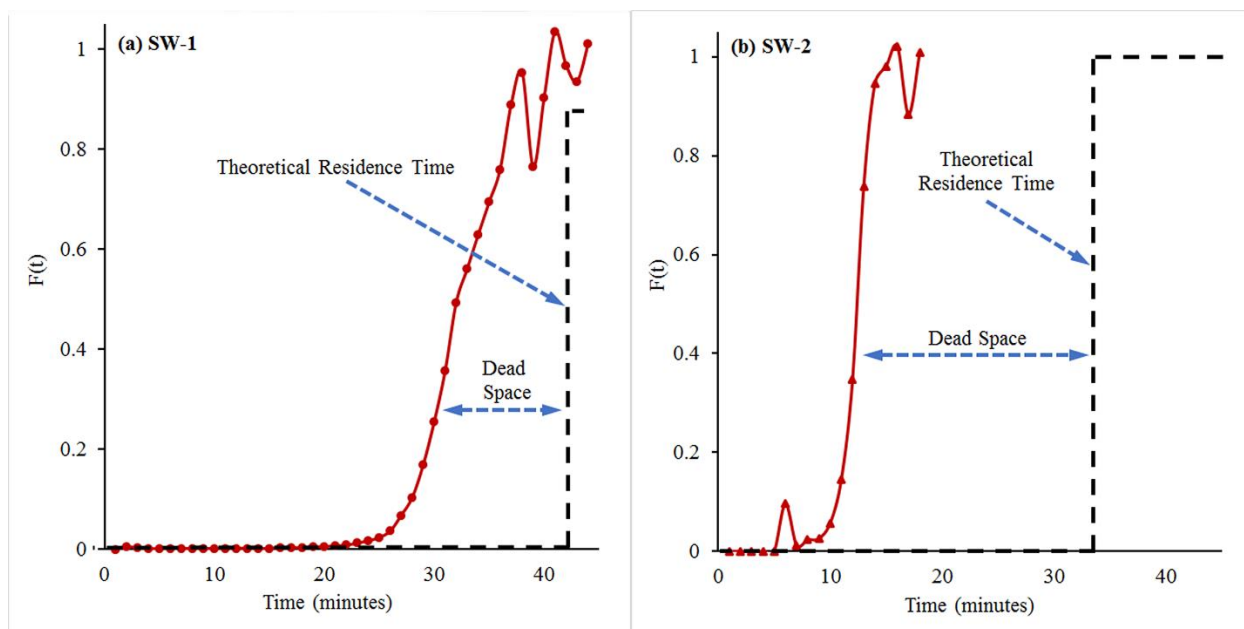


Figure 3: Hydraulic residence time distribution results reveal flow dead space within the reactors. The y -axis represents the ratio of influent concentration to effluent concentration of the step influent tracer. The time difference between the theoretical (vertical dashes) and experimental (dotted lines) breakthrough curves is evidence of dead space, while the skewness of the data is evidence of dispersion within the near-PFR reactors.

In this study, SW-1 was considered loosely packed with an electrode packing density of $350 \text{ m}^2/\text{m}^3$, while SW-2 was considered tightly packed a packing density of $700 \text{ m}^2/\text{m}^3$. Higher amounts of electrode provide more surface area for reactions to take place. RTD analysis showed that the increase in electrode packing density led to a less space-efficient design. The electrode in SW-2 completely filled the anode space while the smaller amount of electrode in SW-1 did not. Therefore, the anolyte in SW-2 had to travel through the electrode material or find ways around it in narrow open channels. Those channels were likely fewer in SW-2 than SW-1, which led to higher amounts of dead volume in the more tightly packed SW-2.

Dead space and dispersion are deviations from ideal PFR behavior that reduce the total expected substrate removal and rate of reaction, respectively, in wastewater treatment reactors. In swMFCs, however, dead space and dispersion are likely to also affect total power production, if not volumetric power density. It is therefore essential to reduce the dead space within the reactors to minimize the fraction of substrate consumption that does not contribute to power production and maximize overall performance. Based on hydraulics data alone it would seem that SW-2 has far too much problematic dead space to be the ideal design, however, as is shown in later sections, substrate removal and power production did not suffer in the hydraulically strained SW-2.

Power Production

The spirally-wound configuration allows high (S/V) ratio, which led to high volumetric power density compared with other configurations. The reactors were operated for more than 3 months, and fig. 4 shows that the voltage outputs were stable for both reactors under continuous flow operation. Fig. 5 shows that at an HRT of 20 minutes (HRT is based on total anode volume of 30 mL), P_{theor} and P_{eff} for SW-1 were $33 \text{ W}/\text{m}^3_{\text{theor}}$ and $51 \text{ W}/\text{m}^3_{\text{eff}}$, respectively. SW-2 produced higher power due to its

compacter design and smaller volume, with a P_{theor} of $51 \text{ W/m}^3_{\text{total}}$ and P_{eff} of $170 \text{ W/m}^3_{\text{eff}}$. The 40 min HRT showed a similar result and trend. The effective power output was calculated based on real flow space, and this metric indicates that SW-2 produced drastically more power in the active anode volume available than SW-1, which would have otherwise gone unnoticed in the absence of hydraulic characterization.

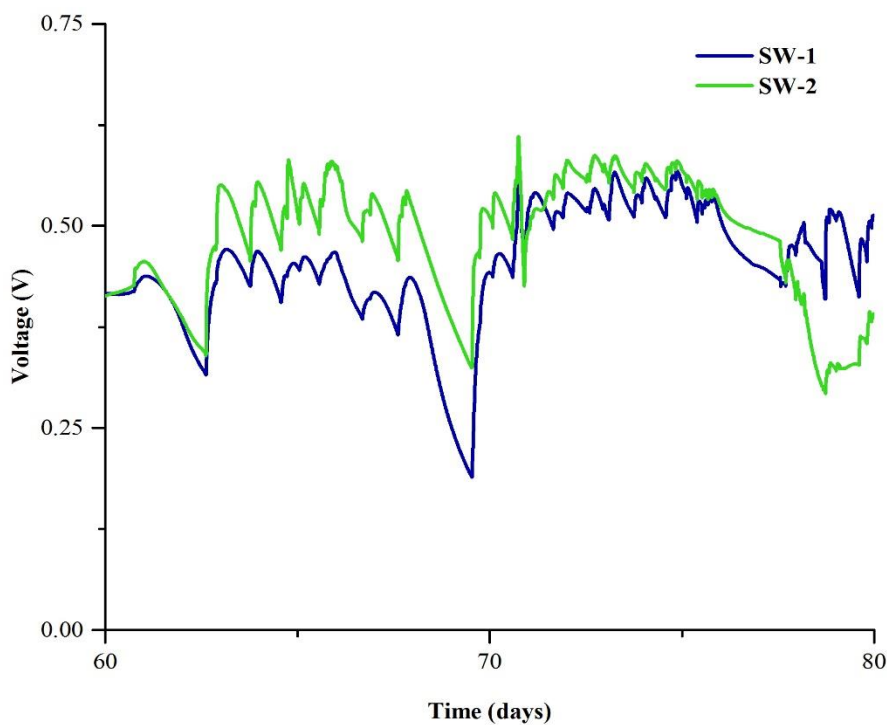


Figure 4: Voltage profile of the two continuous flow swMFCs.

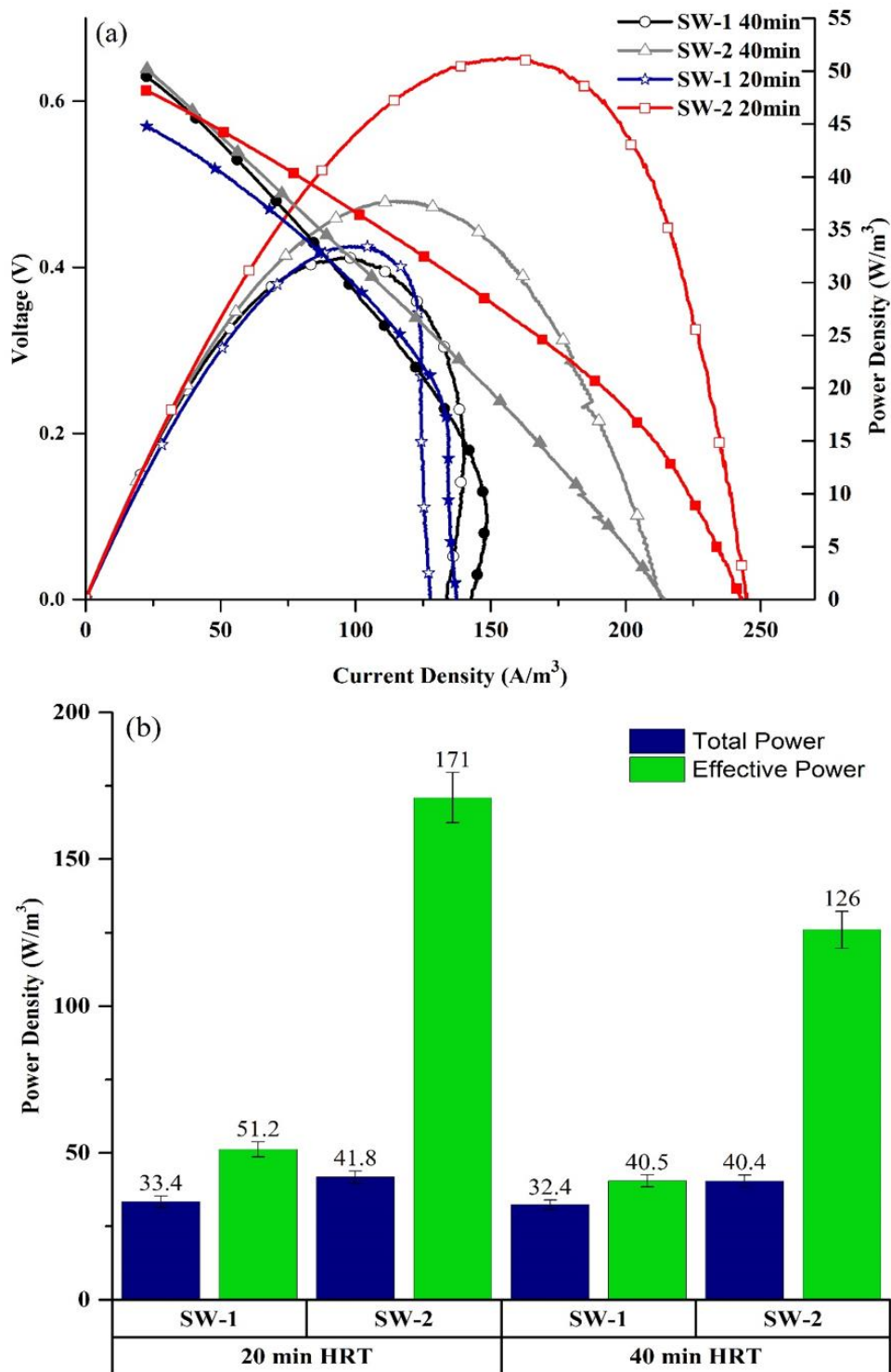


Figure 5: *Power output*: (a) linear sweep voltammetry results showing polarization and power density curves of two different HRTs (20 min vs. 40 min) and two differently packed swMFCs (SW-1 vs. SW-2). (b) Power density comparison. Total power density is based on total anodic liquid volume, while effective power density is based on actual anodic flow space as calculated through hydraulic RTD tests.

The results indicate that a more tightly packed anode allows for higher electrode surface area utilization. Tight anode packing likely forced anolyte through the electrode in SW-2, while the loosely packed anode of SW-1 likely allowed more anolyte to flow around the electrode material. Despite having substantially lower effective volume, the anolyte was more likely to interact with electrode material in SW-2 than SW-1, which boosted power production. Combining power and RTD results, the study suggests that if dead space is reduced while volumetric power density stays constant, the total power produced by SW-2 can be increased by over 200%.

Internal Resistance Characterization

Fig. 6 presents the distribution of internal resistance between the two categories of ohmic and combined charge transfer and diffusion resistance. SW-2 achieved the lowest ohmic resistance of 0.94Ω , presumably due to the close electrode spacing, which was 0.8mm, across the CEM. The narrow spacing also reduced ion transfer resistance in the liquid, resulting in minimal ohmic loss despite low buffer (50 mM) concentration. Ohmic resistance decreased slightly with increasing anode flow rate for both swMFCs. Charge transfer and diffusion resistances accounted for between 49Ω and 55Ω of the total resistances. This study did not go into depth in determining the breakdown of this part of internal resistance, because it was not possible to insert a reference electrode into the very narrow channels, but it was believed that high activation over-potential and charge transfer loss at the cathode was the main contributor to total internal resistance, because no precious metal catalyst was used for the oxygen reduction reaction. A high cathode recirculation rate was employed and cathode diffusion resistance was not likely a major player. The internal resistance data provided here can guide future research to determine the distribution of internal resistance between various components in swMFCs.

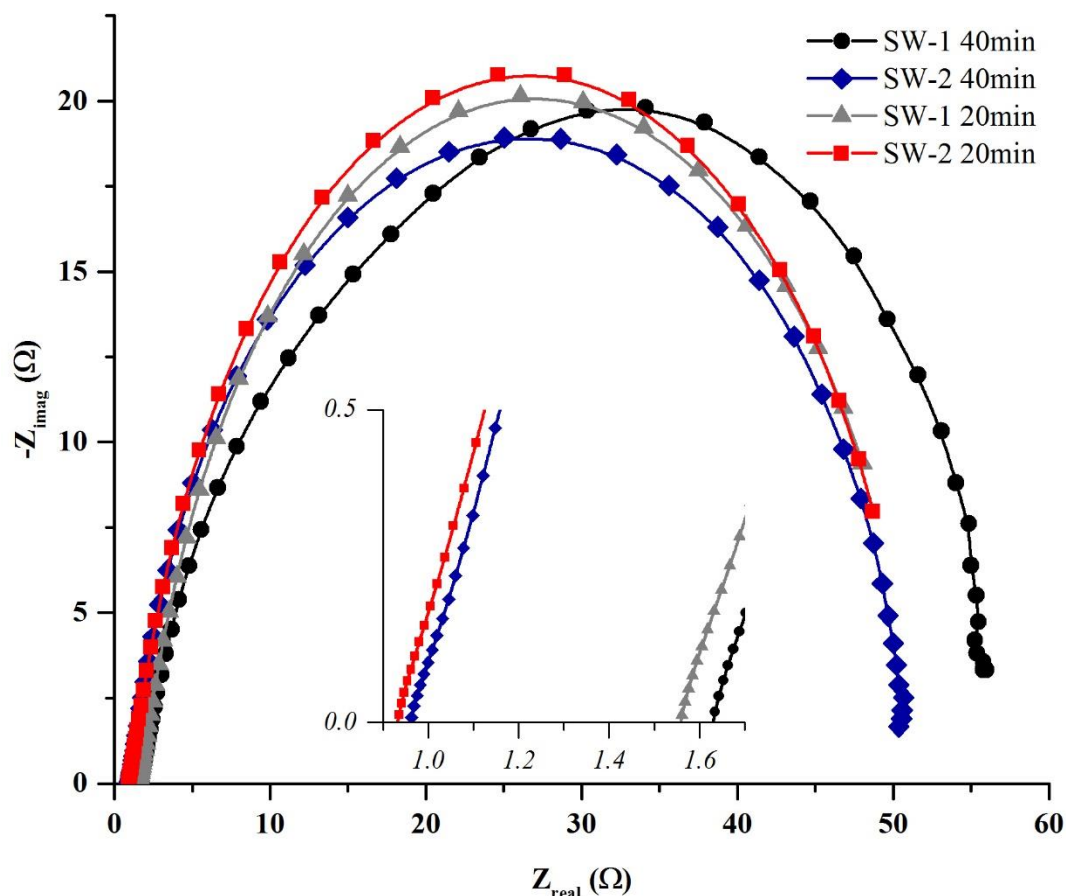


Figure 6: Nyquist plots show low ohmic resistances in the swMFCs and relatively high activation and charge transfer resistances at HRTs of 20 and 40 min (based on total anode volume).

COD Removal and Coulombic Efficiency

Fig. 7 shows the COD removal rates and Coulombic efficiencies of both swMFCs under 3 different flow rates of 0.2, 0.7, and 1.4 mL/min with the corresponding HRTs of 150, 40, and 20 minutes, respectively, based on total anode volume. While both swMFCs were operated at 400Ω, the higher power producing SW-2 achieved a maximum COD reduction rate of 9.01 kgCOD/m³day, which was 4 times higher than SW-1 (2.21 kgCOD/m³day). Despite a lower COD reduction rate, SW-1 showed a higher maximum Coulombic efficiency of 35.8% compared to 19.6% in SW-2. The faster degradation rate in SW-2 should be partially attributed to the larger surface electrode area, which presumably had higher microbial metabolisms. SW-2

also had a lower effective anode volume and concentration polarization was likely less prevalent, which also allowed for higher overall COD reduction rates.

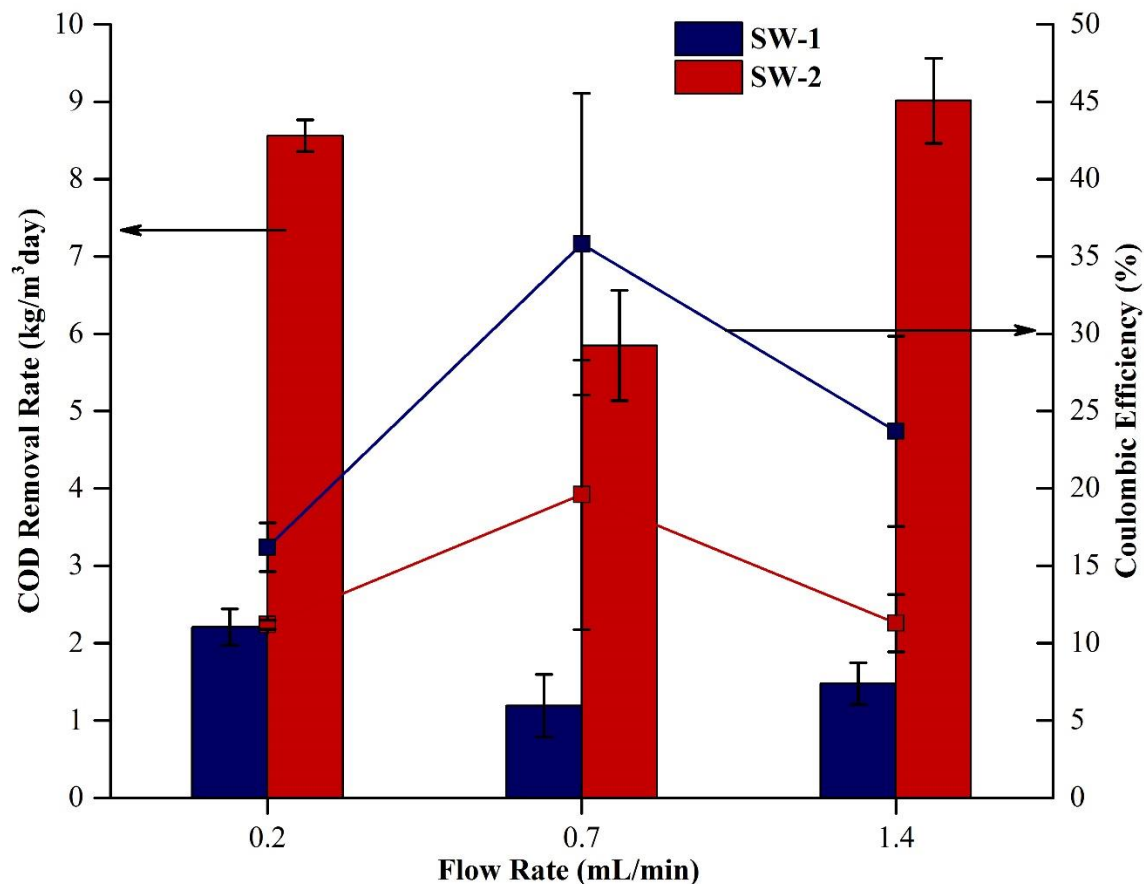


Figure 7: *COD and Coulombic efficiency*: COD removal rates (bars) and Coulombic efficiencies (lines) obtained by the 2 swMFCs under different flow rates. SW-2 removed COD at a faster rate than SW-1, while SW-1 achieved a higher Coulombic efficiency.

Spiral-wound BES Outlook

The spiral-wound design represents a new approach for microbial fuel cell scale-up as modular systems. Taking advantages of compact, modular, and high performing designs that have been proven in water reuse practices, such configuration can be suitable for many industrial and military applications. Traditionally the difficulties in manufacturing such devices are the main barrier, but

the proof of concept for consistent and tightly-wound swMFCs presented here should provide more confidence and capability for system optimization. Air-cathode swMFCs can be developed to minimize the usage of catholyte chemicals, but careful designs to facilitate oxygen reduction reaction while reducing catalyst cost need to be investigated. Separators will still play an important role to limit oxygen inhibition on anodic exoelectrogens. Devices with more than two chambers are also desirable for their capacity to perform advanced processes such as desalination, but represent a higher level of complexity. While the reactors were operated for over 3 months without clogging or noticeable performance decreases, future long-term studies should be conducted to determine the effects of parameter changes and material buildups on system performance and microbial activities.

Conclusions

The compact configuration of the spiral-wound MFC yields high S/V ratios and the devices built in this study demonstrated high power output without using expensive metal catalysts. Contrary to other small scale MFCs with high power output, the swMFC can be manufactured in a modular fashion and scaled for different applications. The hydraulic RTD tool allows the identification of non-optimal flow distribution and therefore offers a valuable approach for system design and optimization. Further research is needed to optimize hydraulic performance with principal focus on dead space as well as power production through the analysis of cathode behavior. While there is room for improvement in the swMFC, the spiral-wound configuration can be applied to other BES such as the MCD relatively easily with the manufacturing knowledge gained in this study. MCD is more complex than MFCs and has expanded treatment abilities with the inclusion of a third desalination chamber. The dual-function of MCD for organic and salt removal fills an emerging

niche in the oil and gas produced water treatment market and as will be shown in chapter 3 spiral-wound MCDs are feasible and preliminary results from their operation will be presented.

CHAPTER III

OIL AND GAS PRODUCED WATER TREATMENT WITH SPIRAL-WOUND MICROBIAL CAPACITIVE DEIONIZATION

Introduction

The development of unconventional oil and gas plays in North America has had dramatic impacts on economic growth, environmental stewardship, and social consciousness. In the United States wastewater generated from oil and gas exploration and production has been estimated to exceed 21 billion barrels per year and is generally referred to as produced or flowback water (C.E. Clark 2009). The composition of produced water and flowback water is highly variable between wells and formations and also over the life of a well. Oils, suspended solids, dissolved solids and dissolved organic matter fluctuate depending upon the age of the well and the geological formation. Total dissolved solid concentration can range from 1 g/L to 400 g/L and dissolved organic carbon can range from 10 mg/L to 4000 mg/L. (ref) Contaminants present and their variability make treatment with conventional methods difficult and cost-prohibitive. Over 2 billion gallons of brine, 90% of which is oil and gas wastewater, are injected into the approximately 144,000 class II injection wells in the United States (USEPA 2012). Well injection has been linked to seismic activity and is a burden on transportation infrastructure (Keranen et al. 2014). Technologies such as reverse osmosis, ozonation, electrocoagulation, and low temperature distillation are feasible for produced water treatment, but none are well-established because treatment still isn't cost effective compared to well injection.

Treatment and transportation represent a large portion of energy and cost associated with produced water treatment. BES present a unique solution to the energy costs of produced water treatment since they can convert the chemical energy in wastewater to electricity, and with modification to the standard MFC design, they are capable of simultaneous desalination as well. One of these systems called microbial capacitive desalination (MCD) has successfully been used on a small scale with real produced water to remove 66% of the dissolved organic and 85% of the dissolved salts while generating additional usable electricity (Forrestal et al. 2015). At this time only a few BESs have been scaled to volumes larger than a few milliliters. The problem with scaling BES systems mainly falls into two areas, reactor configuration and scaling the cathode electrode. Spiral-wound BES configurations appear to have great promise for their high surface area to volume ratios, low internal resistance (Haeger et al. 2014). However, the spiral-wound design does not lend itself to be easily used with the most common cathode electrode used in BES, the air cathode. To address this challenge a new cathode/catholyte paradigm was developed using activated carbon cloth as the electron donor and sodium percarbonate as the terminal electron acceptor (Forrestal, Huang, and Ren 2014). Additionally, since the publication of the MCD system using real produced water, the technology has been improved by modifying the membrane configuration within the MCD system to allow for simultaneous desalination of all chambers of the MCD and increase total salt removal capacity (Ma et al. 2015). In this study, a prototype pilot scale system using the improved MCD technology in a spiral-wound configuration with sodium percarbonate as the electron acceptor was developed for the removal of dissolved salts and organics and energy production from real flowback and produced water.

Background

MCD is a three chambered system that resembles a two chambered MFC with a third desalination chamber between the MFC anode and cathode. The central chamber houses a pair of electrodes for capacitive deionization (CDI). CDI is a system that can remove salts, metals, and other charged species from solution while storing the removed materials on a pair of porous capacitive electrodes (Suss et al. 2012, Oren 2008, Welgemoed and Schutte 2005). Electrode materials are usually carbon-based, including graphene, carbon aerogel, activated carbon cloth, felt, and powder, and hierarchical carbon aerogels (Porada et al. 2013). Less porous materials such as carbon aerogels require a flow-by hydraulic pattern where influent water flows parallel to the electrode plane. More porous materials such as carbon cloth and felt are better suited for a flow-through pattern, which is characterized by flow perpendicular to the electrode plane. Flow-through mode is not recommended for waters high in particulates because there is a higher propensity for clogging and CDI must be designed with consideration for the desired electrode, reactor configuration, and expected influent composition (Porada et al. 2013).

During CDI operation the system is either in desalination mode or regeneration mode. In desalination mode, a potential is applied across the electrode pair and a positive potential results on the anode electrode while a negative potential results on the cathode electrode. The electrodes attract counterions, ions with charge opposite to that of the electrode polarity, and repel co-ions, ions with similar charge to the electrode. Repelling co-ions from within the pore space requires energy just as attracting counterions does so the current efficiency for ion removal is generally below 100%. To reduce current scavenging from co-ion transport, ion-exchange membranes have been integrated between the CDI electrodes as a barrier to co-ion transport and associated energy losses (Biesheuvel and Wal 2010, Lee et al. 2006). Fig. 8a presents desalination mode for CDI in a two-electrode system.

A major benefit of CDI is that the electrodes can be regenerated periodically by reversing the applied desalination voltage or by short-circuiting the electrodes. Reverse-voltage regeneration can be faster than short-circuit regeneration, but is not usually applied in membrane-free CDI due to ion re-adsorption onto the electrodes (Porada et al. 2013). As presented in fig. 8b, ions are released back into solution during regeneration to create a concentrated brine solution. During regeneration the polarity of the electrodes reverse as ions desorb and the current produced during this process can be harvested and reused for consecutive desalination cycles. If desirable materials are present in the feed stream, such as nutrients or metals, the concentrated regeneration solution can be harvested to recover the materials.

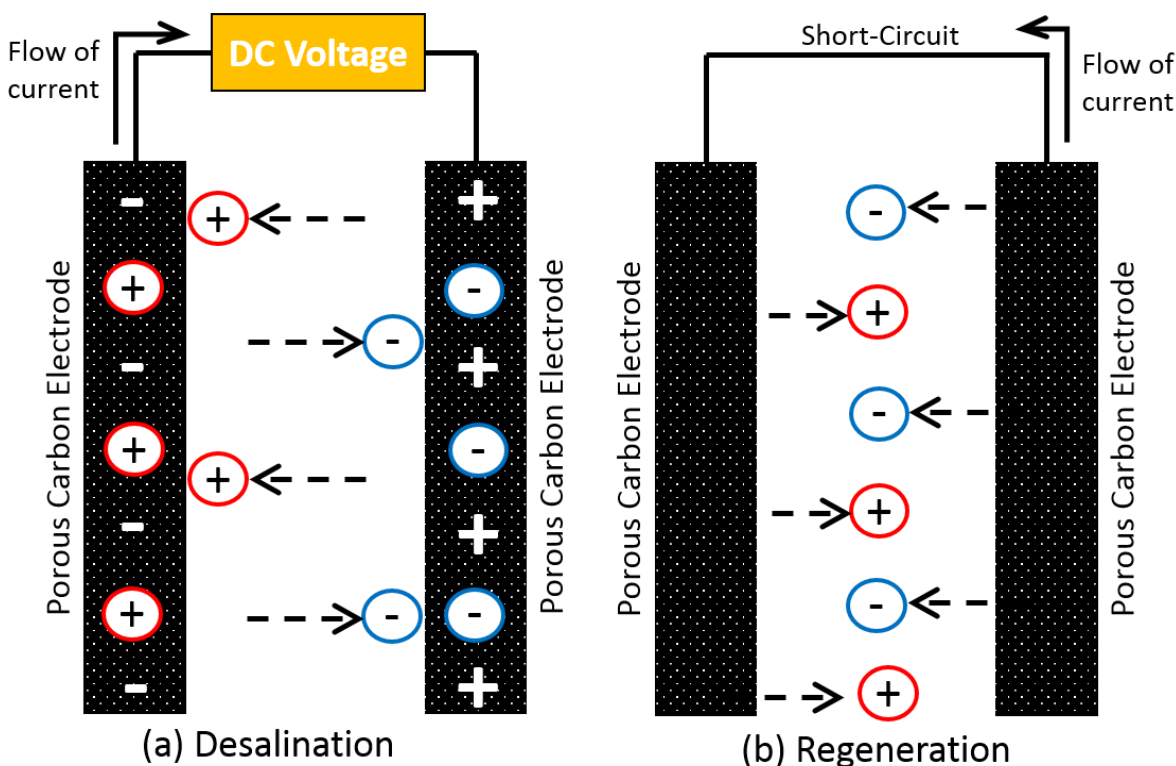


Figure 8: CDI has two operational modes: desalination and regeneration. During desalination (a), voltage is applied across a pair of electrodes to draw counterions out of solution. After the electrodes are saturated, regeneration (b) is carried out by removing the potential and is accelerated by short-circuiting the electrodes or applying reverse voltage.

The combination of CDI and MFC technology is promising for its ability to remove organics and salts without external energy input. The MFC portion of MCD operates as explained in Chapter 2, but the external circuit is replaced by a CDI module. In this configuration, CDI is driven by MFC power derived from organics in the water being treated. The physical connection of the two devices allows ions to be removed from not only in the CDI but also the anode and cathode chambers of the MFC. To maintain MFC function, the anode and cathode are separated from the CDI with either cation exchange membrane (CEM) or anion exchange membrane (AEM).

Spiral-Wound MCD Design

Fig. 9 is a schematic drawing of the MCD system used in this study, but configured as the first MCD study. The configuration used was a cuboid, or a rectangular box shape, formed by rigid acrylic plastic. Such a configuration is very common to BES studies because the acrylic parts can be reused many times and can be combined to form any number of chambers with variable size. As is explained in detail in the previous chapter, the standard design is not easily scaled for a number of reasons. MCD presents a unique set of issues in scaling up. First, its three chamber design requires there to be a CDI chamber between each anode and cathode. With this set of layers, stacking cuboids together becomes uneconomical because of the need for an air-cathode for each anode. If a chemical cathode is desired, stacks can be manufactured without need for a gap for each air cathode, but this type of configuration has proven perilous to manufacture time and time again due to uneven seals and leaking. Using the manufacturing methods developed in Chapter 2, a second sealed off packet can be constructed with relative ease, leaving the space between the two packets for the CDI chamber.

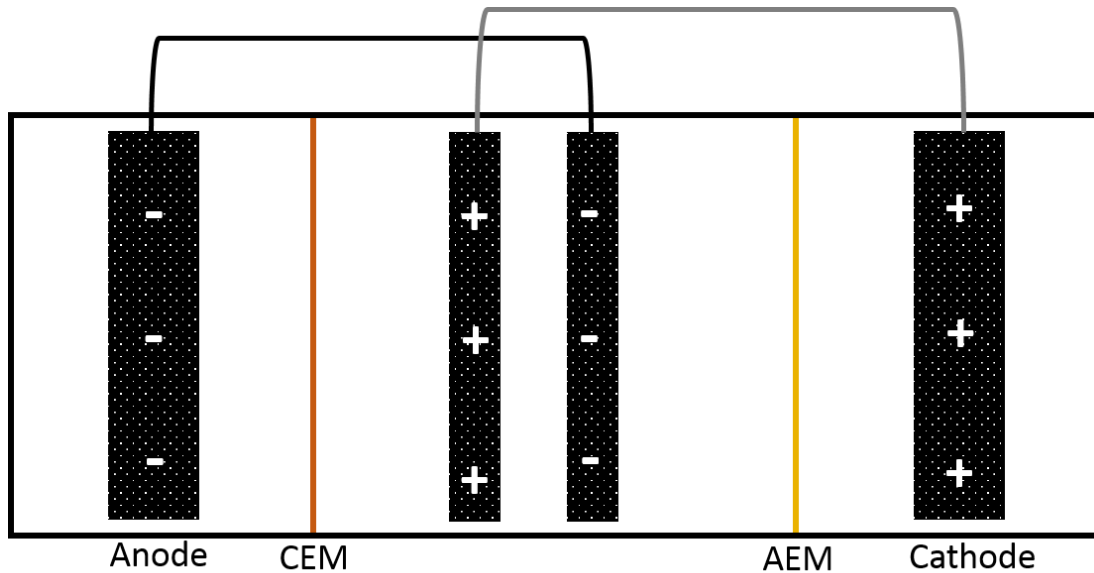


Figure 9: The standard cuboid configuration used in lab-scale experiments. This configuration is ideal for testing electrodes, membranes, separators, and other system variables, but is not feasible for scaled-up systems.

The three-chambered swMCD was designed similarly to the swMFC with enclosed chambers made from ion-exchange membrane surrounded by a third chamber bounded by tubular housing. Both the anode and cathode chambers were formed into packets made of electrode material contained within CEM and AEM, respectively. The desalination chamber surrounded the anode and cathode chambers with the CDI electrodes contained within the space between the two sealed packets. As shown in fig. 10, all of the materials for the anode, cathode, and CDI were structurally housed within a central manifold system that served as the hydraulic inlets and outlets for the anode and cathode. A single manifold was selected based on failed small-scale swMCD tests with separate manifolds for influent and effluent flows. Bi-manifold construction for each anode and cathode was attempted, but the chambers were extremely difficult to seal without the balanced structural support of the PVC housing. Further, the end product did not fit well into circular PCV housing. An oval cross-section resulted since the effluent manifold had to be placed at the outside edge of the spiral.

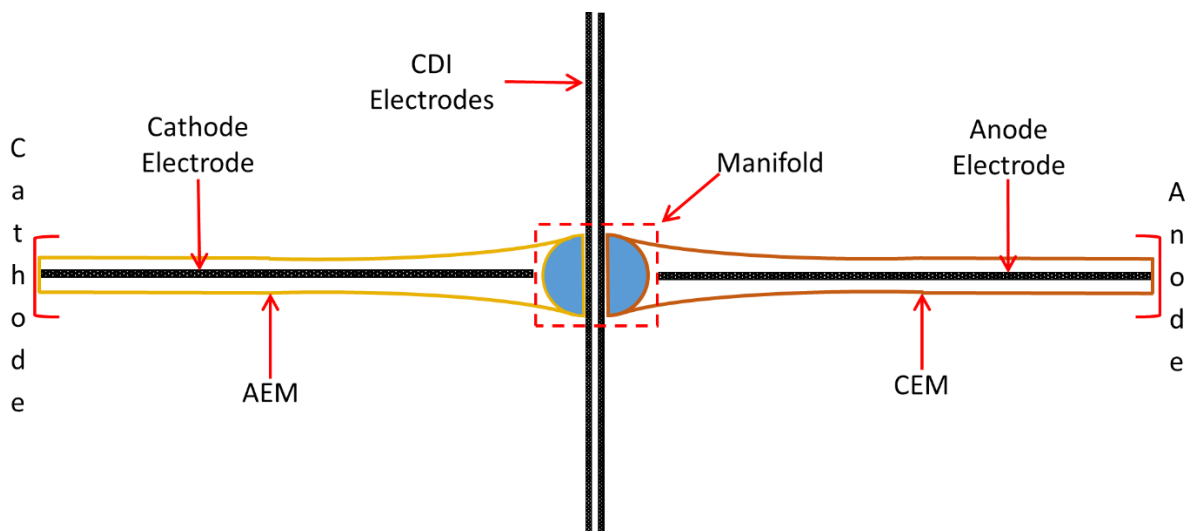


Figure 10: A cross-sectional view of the swMCD materials loaded into the manifold before winding. All materials begin as flat sheets and are wound around the central manifold into spiral form.

A device was built to hold all of the materials and guide them into spiral form for the first attempts at building swMCD. The simple wooden structure is presented in fig. 11a, and fig. 11b is a photo of the structure loaded with materials before adhesive application and winding. PVC manifolds, one for the anode chamber and a second for the cathode chamber, were being investigated at the time of the first swMCDC manufacturability tests. While each chamber had a single manifold, the final spiral was still oval shaped and the final product did not fit into round tubular housing. Furthermore, lack of adequate tension on the materials during the spiral winding process led to problem areas for hydraulic sealing, which are outlined in red in fig. 12. Numerous additional adhesive applications were needed for adequate hydraulic sealing and PVC tubing had to be specially manufactured with an oval cross section to house the swMCD cell. After reactor startup a leak was observed from one of the sealed chambers. It was not possible to remove the swMCD cell from the housing after it was inserted because of the custom construction and the reactor had to be abandoned. While the PVC manifold system was both the least expensive and time-intensive concept compared to other custom-made manifold systems, the

inability to produce hydraulically sealed chambers with circular cross-section led to the abandonment of the design altogether.

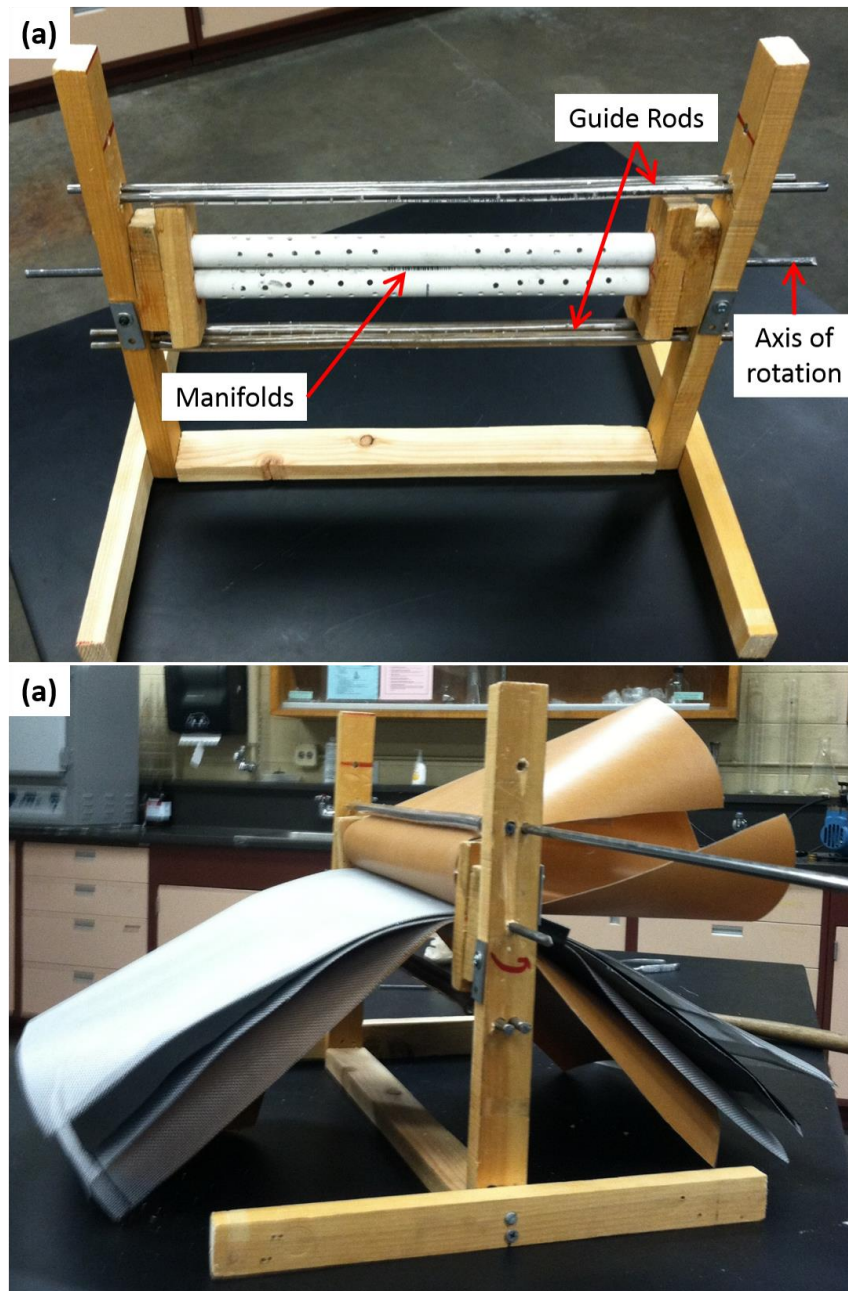


Figure 11: A machine aid was built to house all of the swMCD materials during construction. Winding by hand proved difficult, so the machine was used to wind the materials around the manifolds into spiral form

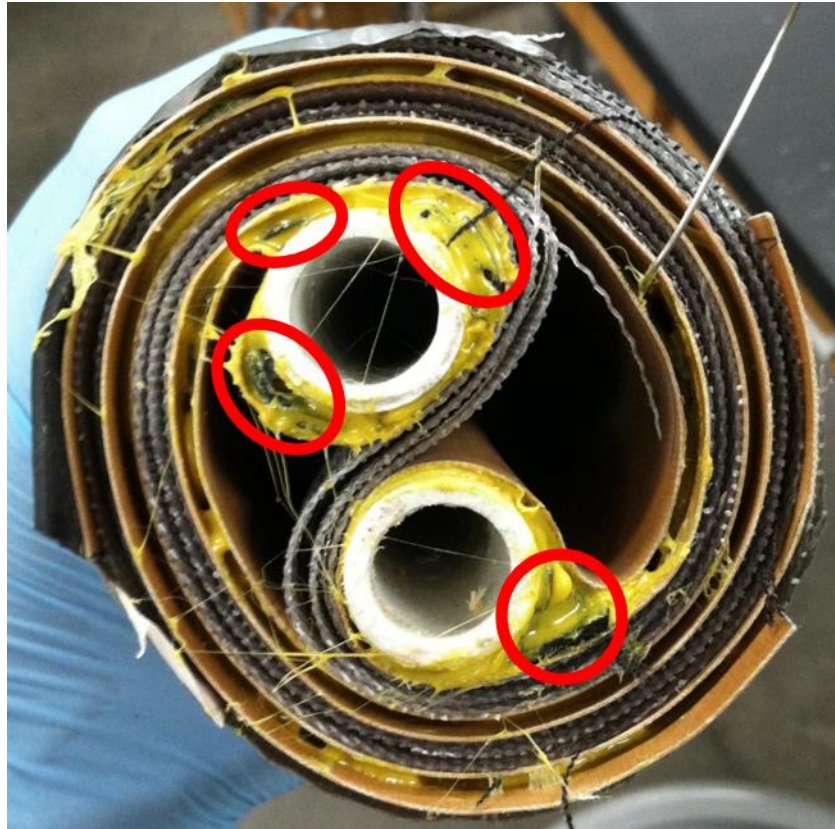


Figure 12: Poor seals formed as a result of both low tension during manufacture and the use of two central manifolds. Outlined in red are areas where major gaps formed, which concentrated near the manifolds.

In subsequent builds the swMCD and the machine aid were redesigned to improve the final product and simplify manufacturing. A single central manifold serving as the hydraulic inlet and outlet for both the anode and cathode as well as structural support for all materials was adopted. One inch diameter polycarbonate rod stock was selected in hopes that the final product would be more circular. Conceptually, as pictured in fig. 10, the solid polycarbonate rod is separated into two halves. One half serves the anode and the other serves the cathode. However, the rod was not cut in half entirely. One inch of solid rod was left at either end of the manifold to hold the materials together and provide points for mounting to the machine aid. The influent and effluent channels for the anode and cathode chambers were routed

out by hand with a plunging router. Machine upgrades included stronger 2"x4" wood construction along with a modified winch to hold tension in the central axis of the spiral during winding. During manufacture, the winch was turned using a wrench and gears inside the winch wound the materials incrementally. Incremental winding was essential for consistent adhesive application while also preventing the spiral from unwinding during manufacture. Also, four guide rods were installed to hold the anode and cathode materials during winding. Two ¼" steel rods were used per chamber and could be compressed around the materials to provide extra tension during winding. The supports parallel to the manifold axis were designed to be easily removed and resized in anticipation of the need to expand the machine to build larger swMCD. Fig. 13 contains a schematic drawing and a picture of the new machine.

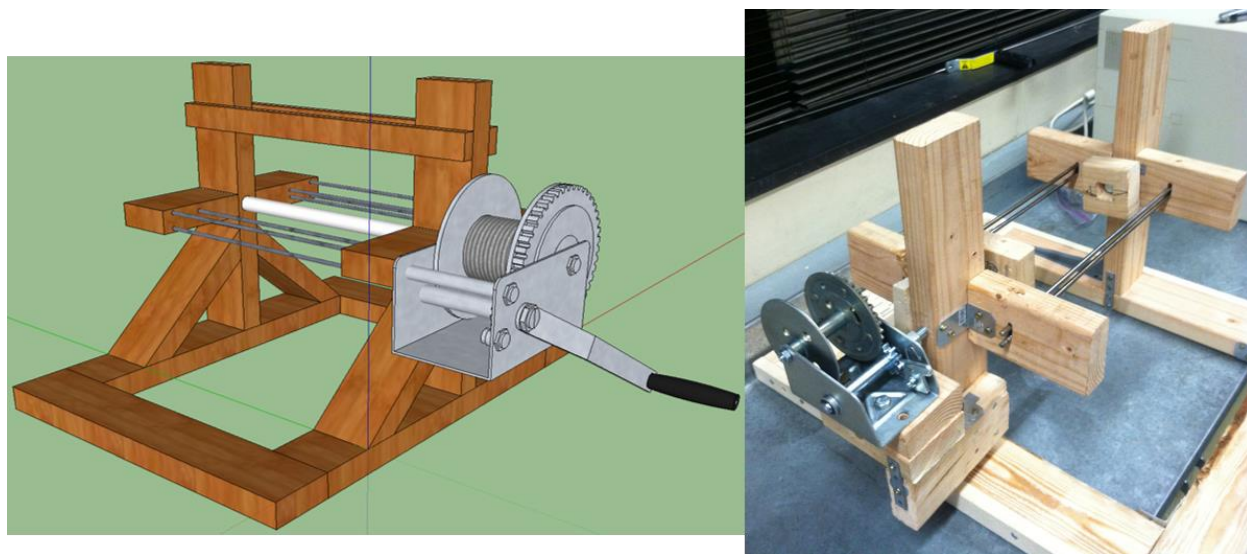


Figure 13: Conceptual drawing (left) and finished machine (right). The winch was connected to the axis of rotation to allow incremental rotation of the spiral while maintaining tension. Tension was provided by the rotational force of the winch pulling against the compression rods (parallel to axis of rotation).

Pilot-Scale Spiral-Wound MCD

Reactor design

The pilot-scale swMCD modules were 39.5" long wrapped around a 41" long 1" diameter polycarbonate manifold. As pictured in fig. 14, the contents and dimensions of the anode and cathode were identical with the exception of the ion exchange membrane used. The anode was surrounded by CEM while the cathode was surrounded by AEM. IEM was sized to incorporate the material surrounding the manifold, around which the IEM was wrapped, and the amount used for each chamber measured 39.5" x 34". A 3/4" gap was left on the three exposed edges of each chamber where 3/4" wide neoprene gasket material was placed. In the center of the chambers, a 1" gap was left for a neoprene gasket measuring 12"x1". A wider 1" gasket was used in the center barrier since it would not be feasible to re-seal this area after the spirals had been wound and sealed. CDI materials were less complicated, with each layer of stainless steel current collector and activated carbon cloth electrode measuring 39.5"x34" and plastic mesh separator measuring 39.5"x40". The CDI, anode, and cathode materials were equal in width at 39.5" so that equal pressure could be applied to the seal areas around the rubber gaskets of the anode and cathode. Solvent-based neoprene gasket sealant was used to bond the neoprene gasket to the IEM, as recommended by an adhesive specialist.

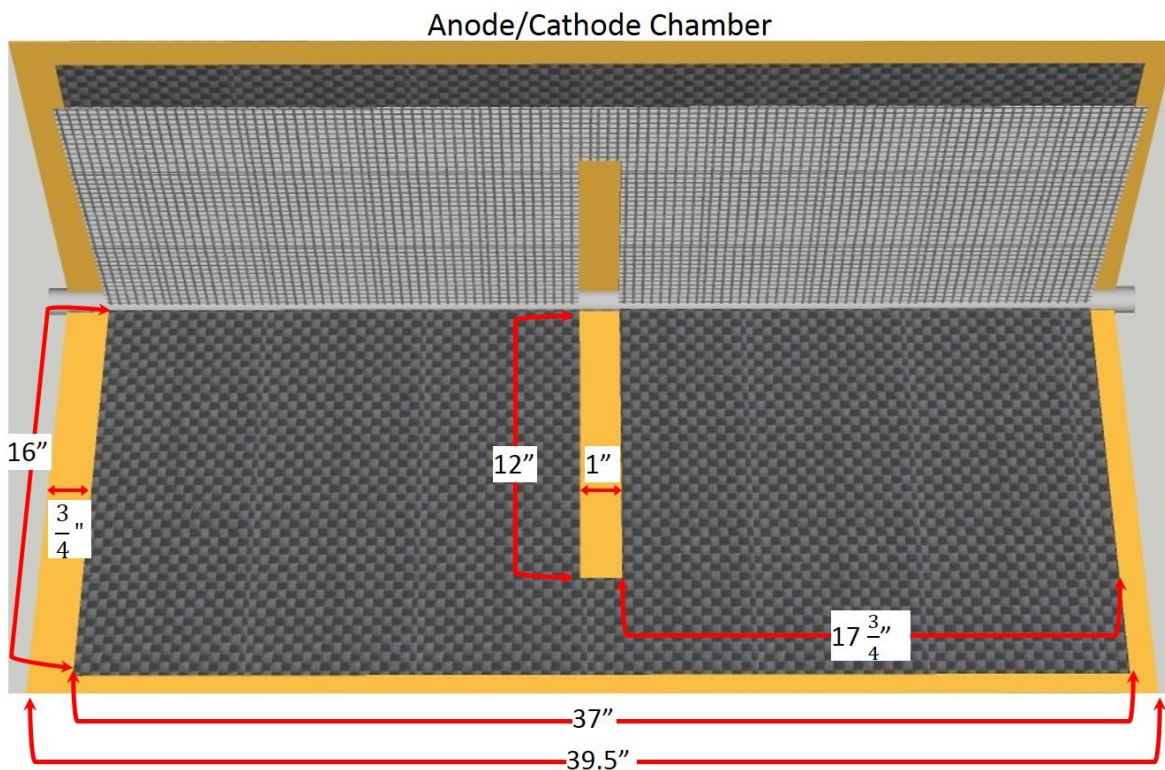


Figure 14: The anode and cathode chambers were formed by folding a single sheet of IEM around a central manifold. Dimensions shown here are for the anode and cathode. The black material is activated carbon cloth and the white and grey checkered material is stainless steel current collector.

Each layer of material as described above and summarized in Table 1 was chosen to maximize contaminant removal, minimize friction losses, and adequately separate the CDI electrodes. The anode and cathode layers selected were as follows (in order): IEM, coarse plastic mesh, activated carbon cloth, stainless steel mesh, activated carbon cloth, coarse plastic mesh, IEM. In the CDI, the layers were as follows (in order): coarse plastic mesh, activated carbon cloth, stainless steel mesh, activated carbon cloth, coarse plastic mesh, fine plastic mesh, coarse plastic mesh, activated carbon cloth, stainless steel mesh, activated carbon cloth, coarse plastic mesh. The CDI was bounded on both sides with the IEM of the anode or cathode and the coarse plastic mesh at the outside edges of the CDI provided a hydraulic flow path. Three layers of plastic mesh were placed between the CDI electrode modules,

which consisted of activated carbon cloth, stainless steel mesh, and activated carbon cloth to prevent electrical connection between modules while also minimizing the electrode separation distance. 16ga insulated copper wire was soldered to the current collectors and liquid electrical tape was used to cover the connections to prevent corrosion.

Chamber	Material	Dimensions
Anode and cathode	Activated carbon cloth	16"x39.5"
	Stainless steel mesh	16"x39.5"
CDI	Activated carbon cloth	34"x39.5"
	Stainless steel mesh	34"x39.5"
	Plastic mesh (coarse and fine)	40"x39.5"

Table 1: Pilot-scale material dimensions

SwMCD Manufacture

The second generation machine aid, as shown in fig. 13, was first resized to accommodate the 41" long manifold and was bolted securely to a benchtop. All materials were loaded into the manifold simultaneously and positioned such that the spiral layers wound exactly on top of one another without overlap on either axial end. Next, several 5mL syringes with tapered tips were filled with the adhesive to prevent the need to refill any syringes during manufacture. All neoprene gasket material was cut to size and roughed with fine sand paper as well. As the winch was turned and materials were wound together, adhesive was applied to all IEM-neoprene interfaces. Adhesive was applied to the anode and cathode simultaneously by a team of two people. The winch was turned incrementally and slowly to allow the adhesive to set for between two and five minutes before pressure was applied. Allowing the adhesive to set provided time for the adhesive to bond to the material and become more viscous.

A more viscous adhesive was less likely to push out from the bond area and was more likely to provide a good seal between materials. When the swMCD was completely wound together, adhesive tape was wound around the spiral to maintain pressure while the neoprene adhesive set. A 24 hour set time was used based on small-scale tests to allow the neoprene to set fully.

After the swMCD set for 24 hours, tap water was pumped through the anode and cathode chambers separately to test for leaks. Additional adhesive applications and the addition of neoprene gasket material were required for both of the two swMCDs built in this portion of the project. Problem areas included the interface between the manifold and IEM, along the spiral edge, and the outer edge parallel to the manifold where imperfect adhesive and pressure was applied. While several repairs had to be made, this method of manufacturing swMCD was successful because sealed chambers were achieved on both swMCDs. When seals were achieved, the swMCDs were loaded into 4" diameter PVC pipe, inlet/outlet ports were drilled through the PVC and connected to the anodes and cathodes, and the CDI chamber ports were drilled through the endcaps of the PVC. In this way, fluids could pass through the anode and cathode separately, and then through the CDI chamber surrounding the two sealed chambers. Finally, the reactors were loaded onto a specially designed 6'x3'x6' (length x width x height) rack system made from 14ga slotted angle steel. A computer, pumps, data logger, and control system was also added to the rack to monitor and control the swMCDs. Fig. 15 contains a photo of a completed MCD reactor and fig. 16 contains a photo of the fully assembled system.

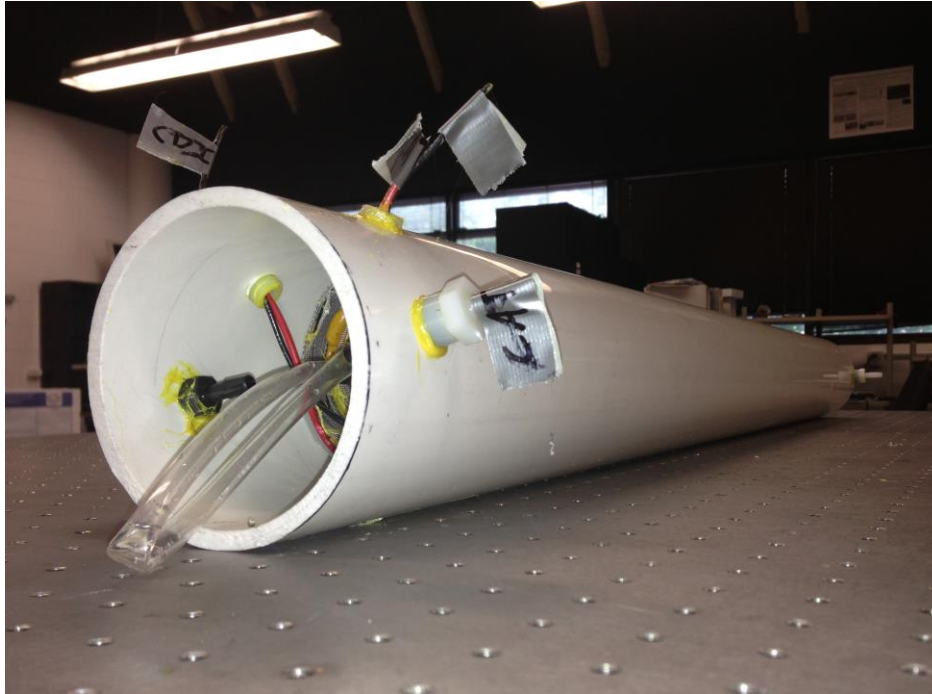


Figure 15: A completed swMCD assembled within PVC housing.

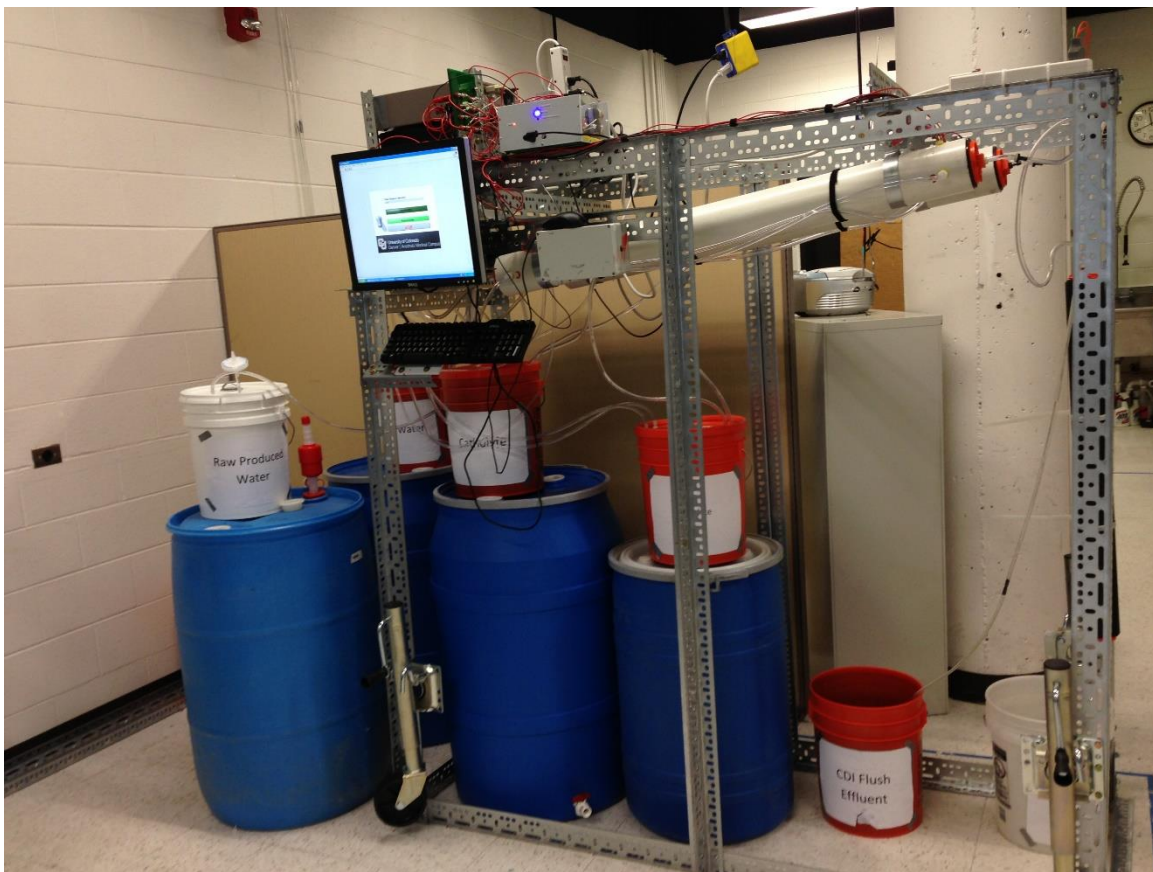


Figure 16: The fully assembled pilot MCD system.

Reactor inoculation and acclimation

Each reactor was acclimated with sodium acetate and sludge to achieve high voltages (>600 mV @1000 ohms). The anolyte contained per liter: 1.6g NaCH₃COO, 0.62 g NH₄Cl, 4.9 g NaH₂PO₄ ·H₂O, 9.2 g Na₂HPO₄, 0.3g KCL, 10ml trace metals, and 10ml vitamin solution. The catholyte solution consisted of sodium percarbonate which contained per liter: 5 g/L 2Na₂CO₃·3H₂O₂, 4.9 g NaH₂PO₄ ·H₂O, 9.2 g Na₂HPO₄. The anode electrode was inoculated with activated sludge from the Broomfield Wastewater Treatment facility (Broomfield, CO) and a 10g/L NaCl solution was in the desalination chamber during acclimation. Following acclimation of the anode electrode the reactors were transitioned to produced water. The microbes in the anode were incrementally exposed to the produced water over several weeks to condition the microbiome to the high salt content of the produced water. Additionally, the cathode and desalination were transitioned to produced water. During experimentation 100% raw produced water was pumped into the anode and cathode chambers, and 4 g/L sodium percarbonate was added to produced water before it was added to cathode chamber.

The reactors acclimated within 2-3 weeks using the artificial solutions. After stable voltage was achieved, the reactors were transitioned to produced water. Because of the high salinity and complex organic constituents of produced water, a sudden transition to 100% produced water was expected to have major negative effects on the microbial anode. Instead, a transition period of two months was used to ease the anode environment onto produced water. When stable voltage over 600 mV was achieved, the reactors were deemed acclimated to produced water. Unfortunately one reactor had to be taken offline after an irreparable leak formed in one of the chamber. The data presented here will be for the single functioning reactor

only. Fig. 17 presents the acclimation voltage data over time as the influent transition progressed.

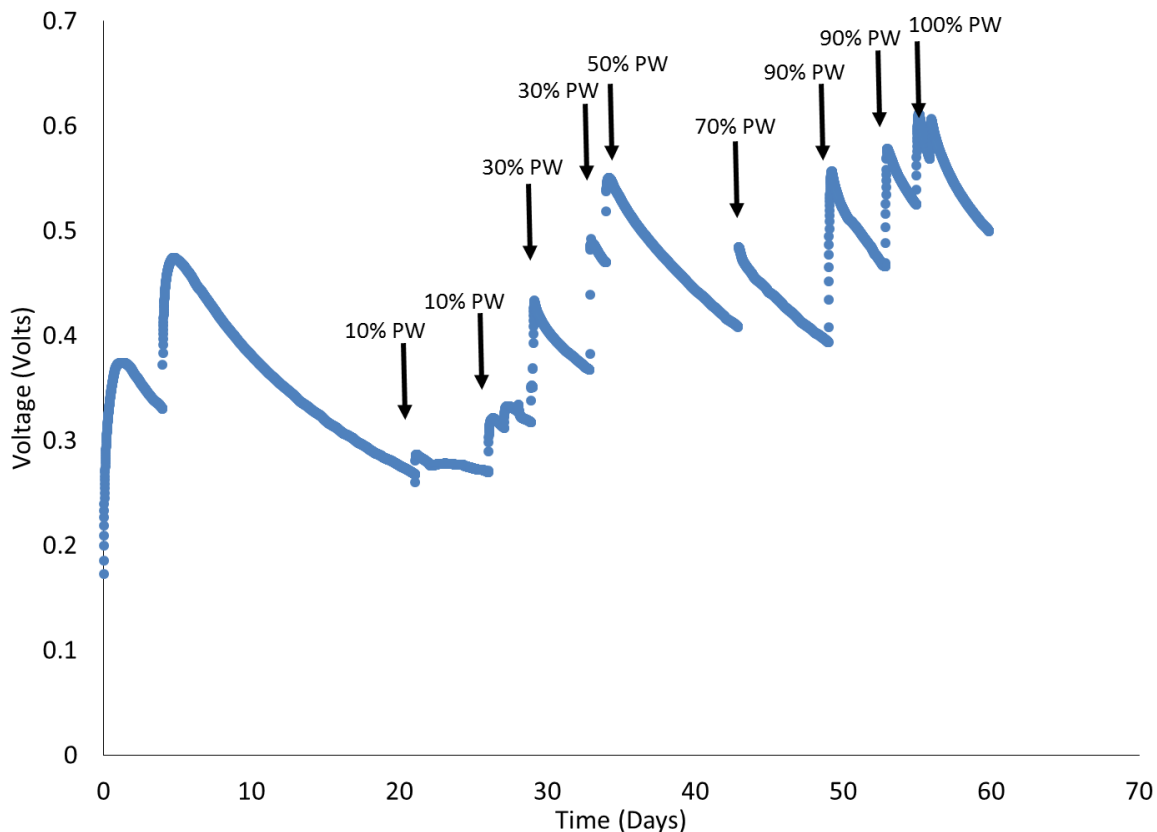


Figure 17: Voltage profiles as the analyte was transitioned to 100% produced water. Over the course of three months, the system voltage stabilized around 0.6V as the microbes acclimated to the saline environment and the biofilm strengthened.

Short-circuiting of the CDI

CDI employs electrode pairs that function as capacitors. As in any capacitor, its performance relies largely on the dielectric between electrodes. If there is good insulation between electrodes, the current added to the device will tend not to leak and the potential difference across the electrodes can be maintained with minimal current loss. If, however, the dielectric fails or there is an electrical short between electrodes, the current required to maintain the potential difference between electrodes is much higher due to current leakage. Therefore, very high resistance, if

not infinite resistance, between the electrode plates is desired for optimal performance. The same principle applies to CDI, however the dielectric between electrode plates is usually saline water instead of an ideal dielectric such as air. Electrode separation distance is one variable that may be modified to minimize the amount of conductive water is between electrode plates in CDI. While minimizing separation distance is desired, electrical short circuits must be avoided.

Electrical shorts were observed between the CDI electrodes of the swMCD after manufacture was completed. Prior to building the swMCDs many tests were run to identify the minimum number of plastic mesh layers and their layering to maximize resistance between plates and minimize separation distance. While the plastic mesh configuration used in the large reactors performed well in a flat-plate configuration, the performance did not translate to the spiral-wound configuration. Manufacturing spiral-wound devices is incredibly difficult and the activated carbon cloth used frays easily when handled. During manufacture, the edges of the CDI electrodes frayed in numerous places, which led to electrical shorts between the two electrodes. It is also possible that the electrode material was extruded through the plastic mesh under the winding pressure and electrical shorts may have formed in this fashion as well. Electrical resistance between the electrodes was measured as low as 100Ω . At such a dielectric strength, to maintain the desired 1.2V an incredibly large current would be required, which the MFC portion of the system could not supply. Future designs will incorporate better CDI separators, which is a portion of ongoing work being done. Because of the poor CDI electrode performance, external DC power was connected to the CDI electrodes during desalination tests while the MFC electrodes were connected with an external resistance.

Desalination performance and COD removal

The results presented in this section do not emulate MCD performance under conditions for which it was designed, since the CDI had to be powered with an external DC power source. Despite this, the results demonstrate the theory that salts and organics can be removed from all three chambers of the system. In a flow configuration where each chamber was recirculated separately from one another, 27% of the influent salt was removed from the CDI chamber, 12% from the anode chamber, and 19% from the cathode chamber for a total salt removal of 10.2 g TDS/L/day. Similarly, 65%, 75%, and 68% of COD was removed in the anode, desalination, and cathode chambers respectively. Experimental results for COD and salt removal are presented in fig. 18. In the anode chamber, COD is removed by microbial oxidation and converted into electrical current. A Coulombic efficiency of 11% was calculated, and is low likely due to dissolved oxygen in the influent stream. In the field, where a series of swMCD would be employed, the effect of dissolved oxygen in the influent stream will be mitigated in each successive reactor. Removal of COD from the cathode chamber was attributed to oxidation by percarbonate, and removal in the CDI chamber was attributed to electrical adsorption onto the electrodes. The reactor configuration also prevented large pH shifts in the anode, where the pH was only observed to have changed from 6.8 to 7.2.

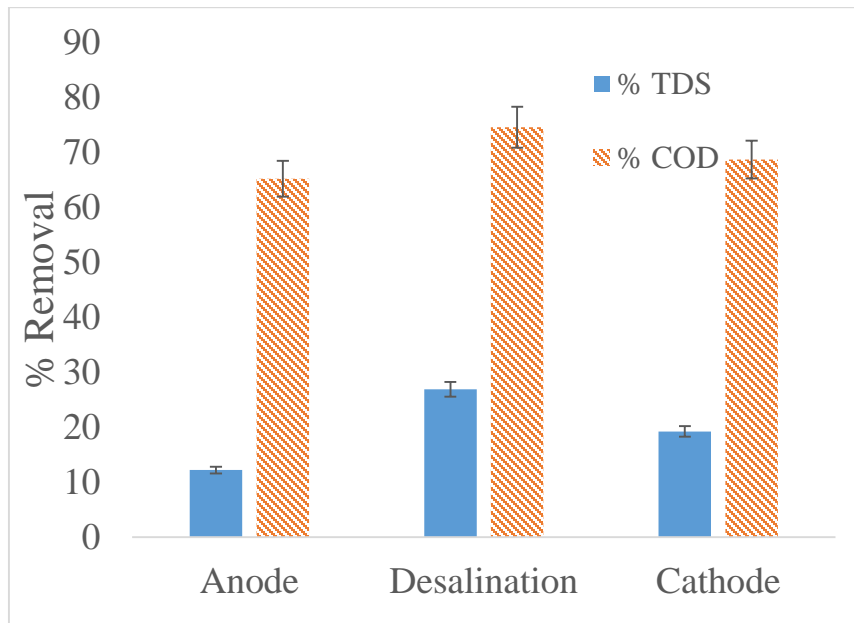


Figure 18: Salts (blue) and COD (red) were successfully removed from all three chambers of the swMCD. Avoiding CDI short-circuiting will improve both COD and TDS removal in future designs.

Power production and internal resistance from BES

To inform possible future design improvements, power production and internal resistance across the BES portion of the swMCD was analyzed. Using linear sweep voltammetry (PC4/300, Gamry Instruments, NJ), it was found that the maximum power point for the reactor was 89 W/m³ based on anode volume and the maximum current production was 228mA. Electrochemical impedance spectroscopy (PC4/300, Gamry Instruments, NJ) showed an incredibly low internal resistance of less than 1Ω, which allowed the higher than average current and power production. The spiral-wound configuration allows for close and consistent electrode spacing, which has been shown to lower internal resistance in BES. Also, the produced water used in these experiments was highly conductive, which has also been shown to improve internal resistance. Fig. 19 presents the linear sweep voltammetry results for the pilot reactor operating on produced water.

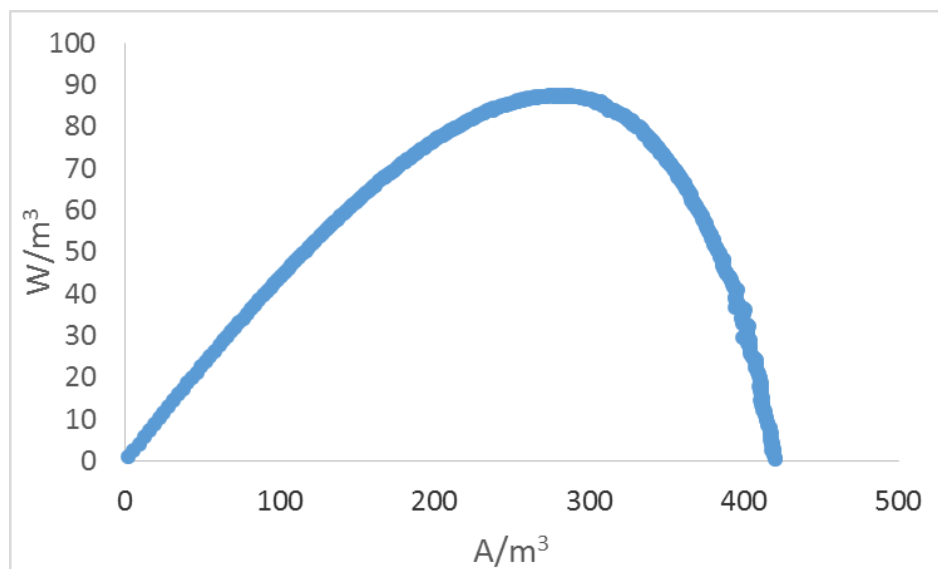


Figure 19: Power density for the pilot reactor operating on produced water

Outlook for large scale swMCD

In this phase of the swMCD the first ever large scale spiral-wound BES was successfully built and tested. High power and current production of 89 W/m³ and 228A respectively were recorded from the BES portion of the swMCD. Coulombic efficiency suffered as a result of 10%-15% dissolved oxygen in the influent stream, but is expected to be less of an issue in larger scale swMCD systems with series of reactors. Internal resistance was among the lowest ever reported in BES, an achievement owed to close electrode spacing and conductive electrolytes. In-depth understanding of manufacturing spiral-wound BES, the aid of a machine, and practice allowed the BES to be built and may be perfected further in the future. An electrically driven winding mechanism would allow for more consistent adhesive application and a lower propensity for seal failures. Stopping adhesive application to turn the winch resulted in errors in adhesive application during manufacture and performing repairs on the seals after manufacture required up to five times the time required for initial manufacture. Finally, while the adhesive used performed the best

out of any tested, no specialized ion-exchange membrane sealant exists. For large scale production a specialized adhesive may need to be developed.

Errors in the CDI portion of the swMCD led to many problems with desalination performance. Short-circuits due to material failure and imperfect manufacturing were at fault. Work is currently being done to identify better CDI electrode separators. Separators being tested include a five layer plastic mesh setup, cation exchange membrane, and solid plastic sheeting. Preliminary tests indicate that all three provide sufficient electrode separation in swMCD and flat-plate form and desalination performance tests are underway. Other work being done includes testing a highly electrically conductive carbon/graphite felt designed for high temperature insulation. The felt material does not fray and is much easier to work with than carbon cloth. It is believed that improving the separator performance while incorporating more workable materials will greatly improve swMCD performance.

CHAPTER IV

AUTOMATION OF BIOELECTROCHEMICAL SYSTEMS AND CAPACITIVE DEIONIZATION FOR LABORATORY AND FIELD APPLICATION

Introduction

The renewed mentality of open sharing and collaboration in the age of the internet has spawned great innovation and product development. A key result of the open source movement is a range of low cost and easy to use microcontrollers that are now used in everything from internet-connected toasters to autonomous drones and other flying machines. Open source microcontrollers have been publicized greatly in the do-it-yourself community, but their use in the engineering community has not received the same attention. The highly functional devices have proven capable of monitoring and controlling a wide range systems from greenhouses to teams of autonomous drones without the need for separate centralized computing systems. Despite having low power requirements, versatility, and proven dependability in distributed applications, the functionality of open source microcontrollers has barely been tapped to date in environmental engineering applications.

Wastewater treatment is a rapidly changing field and a major component of environmental engineering. Many research efforts are actively seeking ways to make wastewater treatment systems more reliable, lower cost, and less energy intensive. As the developing world enters wastewater treatment, communities in these areas will look first for community-scale systems that are low-cost, low-energy, and easily maintained. Developed areas will similarly look for low-cost, low-energy, and reliable

systems to upgrade existing infrastructure. The impracticality of traditional high capital cost and very intricate systems will not be applicable for much longer in an age where environmental conscience is at an all-time high. A promising technology that has the capability to solve many problems in wastewater treatment is the bioelectrochemical system (BES). The BES is a multifunctional platform technology capable of producing electrical power while simultaneously treating a number of types of wastewater. This technology has emerged in the past decade as one of the most promising new wastewater treatment technologies for its capacity to move centralized wastewater treatment systems off of the electrical grid towards energy positive treatment. There is growing interest in decentralized wastewater treatment systems as well in all areas of the world. The electricity produced by BES is likely capable of powering low-energy microcontrollers to make decisions about treatment efficacy. While the use of microcontrollers with BES opens many field applications, their combined use in the laboratory setting can also be very useful.

The first step in the process leading up to deployment of autonomous devices is to test their performance in a controlled setting. In this experiment two automation tests were run. The first test was on automatically controlling the swMFCs presented in chapter two. Percarbonate was used as the catholyte and its oxygen reduction potential was the limiting factor in maintaining maximum power during experimentation. To ensure fresh catholyte was present during acclimation and in the period of time leading to maximum power testing, an automated catholyte replacement system was used. Secondly, a control system was developed for MCD control. The MCD control system was designed to gather data for abiotic system pre-testing to benchmark CDI performance prior to microbial inoculation. Abiotic tests were run to remove microbial power variability between reactors. While basic in

nature, both tests are expected to prove useful in designing future BES and MCD control systems for field deployment.

Automated catholyte replacement controls

Automated controls require feedback that can be correlated to system performance. Voltage output under constant external load is an excellent indicator for BES performance since a well-functioning system will have constant or increasing voltage output while a poorly-functioning system will have inconsistent or decreasing voltage output. Factors affecting voltage output for a given system include organic concentration in the anolyte, pH, temperature, electrolyte conductivity, and catholyte oxidation reduction potential. Voltage shifts indicate system changes and when voltage shifts in the laboratory setting corrective action takes place through human interaction. System changes that affect the power output of BES can occur at any time and even when laboratory personnel are present they often go unnoticed. To maintain optimal performance of reactors for reporting purposes it would be beneficial to implement automation systems that monitor and control system variables at all times. The swMFCs reported in Chapter 2 were operated with automatic catholyte replacement systems to optimize the oxidation reduction potential of the percarbonate catholyte with voltage output as the feedback variable. While catholyte was replaced several times per day to maintain performance, the organic strength of the anolyte solutions used was high enough that they only needed to be replaced every two days.

Experimental setup

In this experiment, an swMFC as described in Chapter 2 and (Haeger et al. 2014) was operated under continuous flow with the solutions described there. Automation was performed by an Arduino Uno R3 microcontroller (Arduino, LLC) to periodically feed catholyte when voltage output began dropping. In each loop of the

main program, voltage is read and compared to the voltage read in the previous time step. If the voltage decrease was greater than 1.1 mV (the precision of the microcontroller) over a two consecutive six minute periods, catholyte replacement was allowed to begin. A 3L reservoir containing 1 g/L sodium percarbonate was located approximately one foot in head above the catholyte inlet to the swMFC. In the catholyte replacement cycle a valve near the catholyte inlet, denoted 1 in fig. 20, was opened and catholyte contained within the reactor was allowed to drain without added pumping through gravity forces into a waste reservoir. Valve 1 was opened for 100 seconds, which was determined experimentally to be sufficient for draining to complete, before closing. Next, valve 2 was opened and fresh catholyte flowed through gravity into the cathode chamber. Valve 2 was left open until a float switch in the top of the cathode chamber communicated to the Arduino that the cathode chamber was full. A second float switch was placed in the bottom of the fresh catholyte reservoir (blue in figure). In the event that the catholyte reservoir was empty the cathode draining function was not allowed to proceed. Also, a button was installed in the microcontroller for use in manually beginning the catholyte replacement cycle. Finally, an LCD display was installed to output information about the state of the system including if the catholyte reservoir was empty, when the cathode was draining, when it was being filled, the current voltage, and the difference between the current and last voltage reads. Each loop of the program was approximately six minutes, with variation coming from the time required to fill and drain the cathode. Programming of the microcontroller and design of the system was done by the author with the aid of open source programming libraries. Appendix A contains the catholyte feeder program in its entirety.

Anolyte is consumed much more slowly than catholyte and a 1L anolyte reservoir, depicted in red in fig. 20, was sufficient to maintain high organic strength

over the course of experimentation. One pump was used to continuously recirculate the anolyte and catholyte, which was not interrupted by the automated catholyte feeding. To further conserve energy, latching solenoids were used as the valves in the experiments. Electromagnetic forces applied through a pulse of DC power to a coil move the valve open or closed depending on the polarity of the applied power. Many designs for latching solenoids exist, but a common design uses one permanent magnet to hold the valve in one position and a spring to aid in reversing the valve position when the electromagnet is activated. By requiring only periodic electricity application, latching solenoids greatly reduce power requirements and problems with heating compared to constant-power solenoids (Savoie 1973). The system was monitored and analyzed by the methods presented in Chapter 2 and (Haeger et al. 2014).

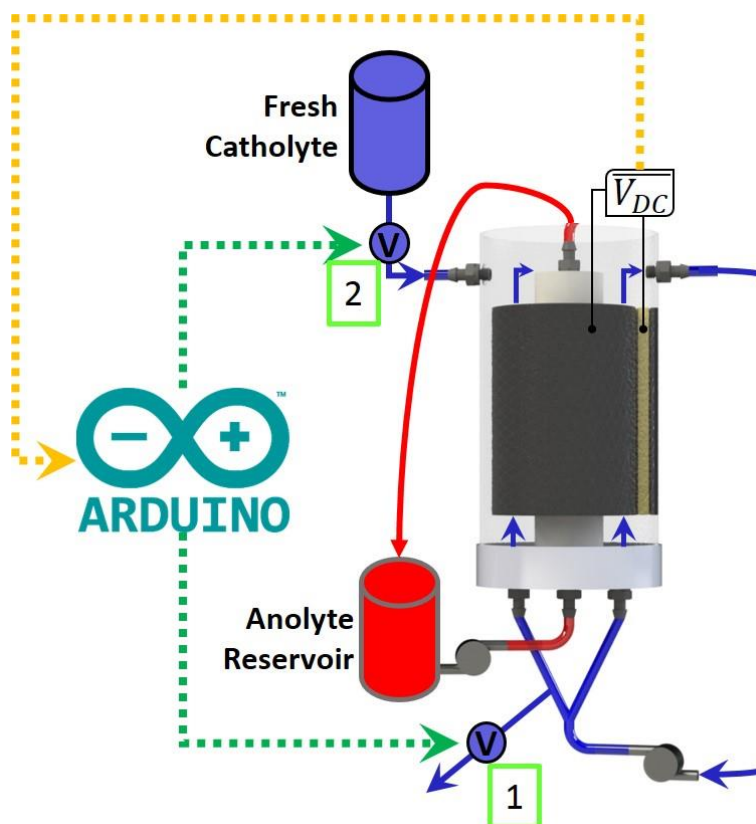


Figure 20: Schematic diagram of hydraulic flows (solid lines) and information flow (dashed lines). Anolyte (red) is recirculated from a 1L holding reservoir. Catholyte (blue) is recirculated through the internal reservoir within the PVC until replacement is needed. During catholyte draining, valve 1 is opened and catholyte flows by gravity into an effluent reservoir. Afterwards, valve 1 closes and valve 2 opens to fill the catholyte reservoir with fresh solution. Voltage (dashed yellow) is read by the Arduino microcontroller and the valves (dashed green) are actuated accordingly.

Results and Discussion

Automated catholyte feeding boosted voltage output in the period leading up to and following power density testing. Power density is an established parameter reported in the literature for BES and it is important to make sure the system is operating optimally before and during the testing period. Preparation of a reactor for power density testing through linear sweep voltammetry is to replace all solutions and allow the system to achieve high voltage output. Next, the reactor is put into open circuit mode and allowed to equilibrate for around two hours. Leading up to removing the external circuit it is possible that the catholyte will be exhausted,

especially when dealing with fast-acting chemicals such as percarbonate. Fig. 21 contains voltage data representative of a reactor being prepared for power density testing. First, anolyte was replaced along with catholyte while the voltage output of the system was round 200 mV. Voltage initially boosted up to around 375 mV within the first 500 minutes before it began to level off. Then, the catholyte feeding system fed three times automatically over the next 1,000 minutes followed by two manual feeds to boost the system to 500 mV. The jump in voltage just before 2,000 minutes is from when the system was put in open circuit mode for power testing. As can be seen by the voltage profiles in fig. 21, without automatic catholyte replenishment the voltage for the system may have levelled off around 400mV before power testing. The automation system provided the MFC system with the highest performing cathode possible for longer than would be possible with periodic manual feeding. Cathode performance is widely accepted to be a bottleneck for MFC power output, and cathode performance is synergistically linked to anode performance. Maintaining the cathode at such a high level in this experiment likely led to a more highly functioning anode as well.

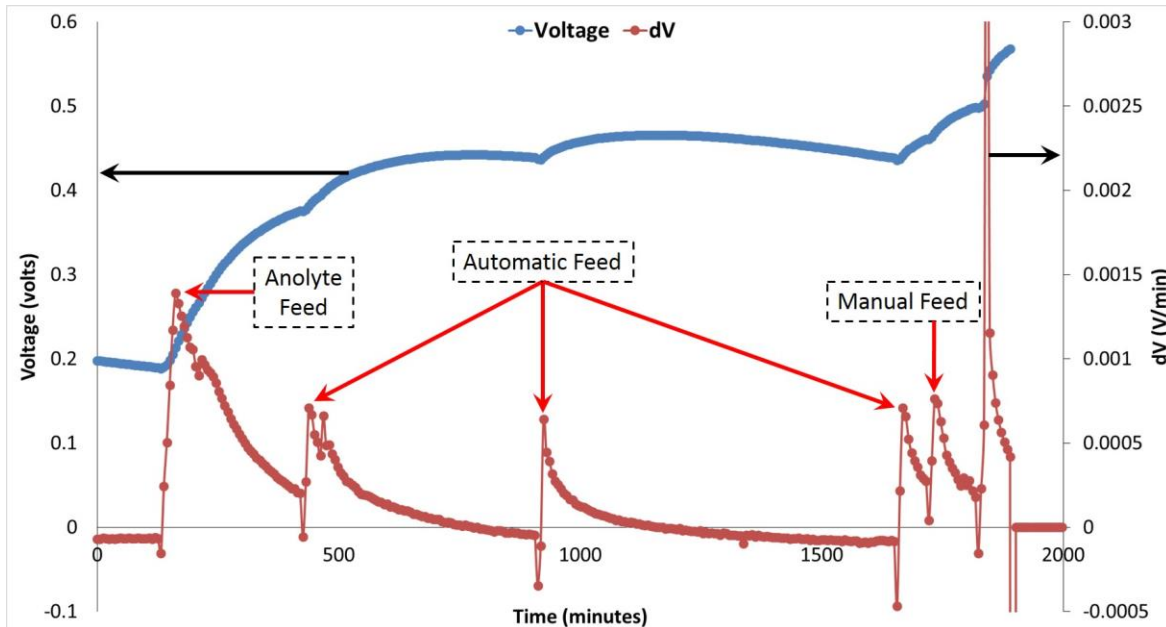


Figure 21: An MFC must be operating optimally before power density tests are run. Anolyte and catholyte are usually replaced simultaneously before testing begins, but with automated catholyte replacement voltage can be boosted to high levels. Over the course of about one day, voltage was boosted from 0.2V to over 0.5V and maintained there until power density testing. Frequent replacement of the catholyte ensured the power density results presented were the highest possible.

After power testing, the external circuit (1,000 Ω resistor) was re-connected and voltage was maintained for over 60 hours without anolyte replenishment. Fig. 22 contains the voltage data for this period, over which catholyte was replaced six times. It was observed that power density increased over time and it is likely that by maintaining high cathode potential and strengthening the exoelectrogenic anode microbiome the automation system accelerated the pace of improvement. Future work should be done to verify this theory, which could not be done in this test for various reasons. Firstly, while it is possible that an automated feeding system boosts power density altogether, tests should be run in the future with simple cuboid reactors that can be built very similar to one another for direct comparison. Boosting voltage with automatic catholyte replacement is also beneficial because it not only reduces the time required to prepare a reactor for power density testing, but also

maintains high voltage output between power density test during which COD removal tests and others can be run under optimal conditions. As shown in fig. 23, when the automation system is idled, system voltage drops as solutions are exhausted.

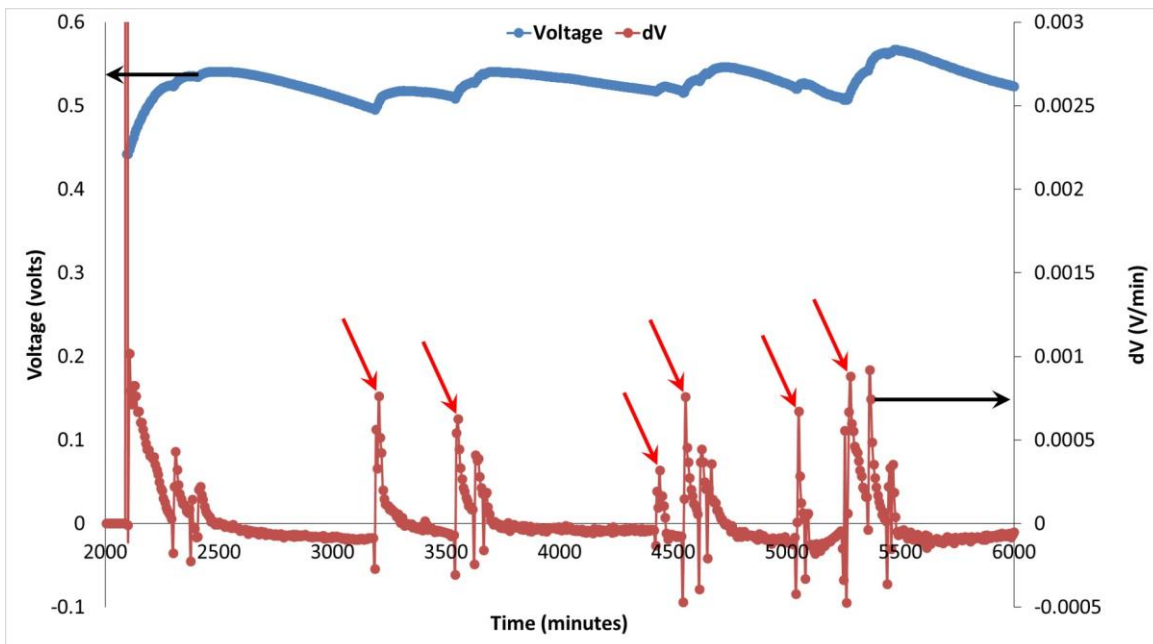


Figure 22: Maintaining high performance over time requires maintaining all electrolytes at optimal concentrations. In this case, the catholyte was the limiting factor. Between power density testing the automated catholyte replacement system maintained system performance for over almost three days without needing to replenish the anolyte.

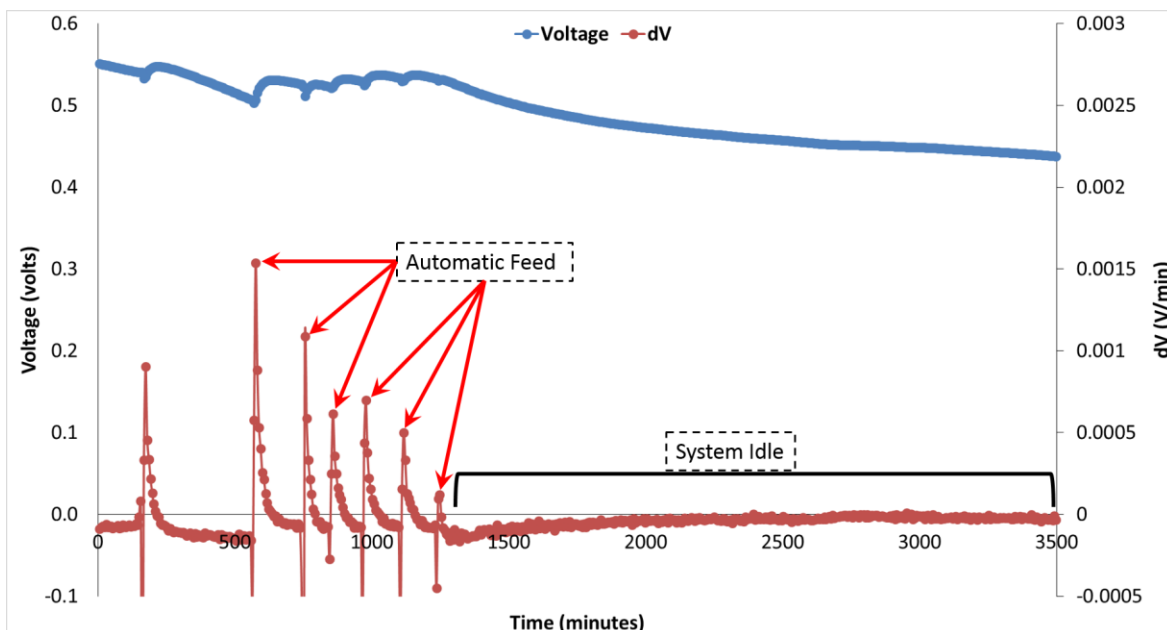


Figure 23: Following putting the automation system into an idle state, system performance drops. The automation system can be adapted to maintain sub-optimal performance in the field to minimize catholyte use while maintaining adequate COD removal and power production.

MCD automation

MCD is a more complex system than MFC and are difficult to operate on any scale. As described in Chapter 3, the MCD system consists of an MFC coupled with a CDI where the power generated by the MFC is used to charge the CDI electrodes. Imprecision resulting from manually switching between states of desalination and regeneration often results in current loss from the CDI and periodic open-circuit operation of the MFC. To maintain the stability of MFC power output and maximize energy harvesting during regeneration, near-instantaneous switching is needed. Further, desalination data must be gathered over many cycles, which can be prohibitively difficult. Readily available benchtop conductivity meters are not easily linked to computers and tend to have small internal data storage capacity. Most devices that do allow constant data gathering are custom-built for large desalination applications and are too expensive for the laboratory setting. Automation is needed

to improve control and data gathering in the laboratory and in scaled up applications. In this study, open source microcontrollers and conductivity circuits were used to control and monitor an abiotic MCD system. Continuous operation was achieved over many days without data loss or need for user input to the control system.

Experimental setup

An MCD was designed and built using a cuboid configuration. The reactor was 3" x $1\frac{3}{16}$ " x $1\frac{3}{16}$ " with internal circular cross section. CDI electrodes were $\frac{1}{4}$ " thick graphite felt (Mersen, France), the anode electrode was $\frac{1}{2}$ " graphite felt (Mersen, France). The air-cathode was prepared according to accepted practices by applying 0.5 mg/cm Pt/C and for PTFE diffusion layers on 30% wet-proofed carbon cloth (Forrestal et al. 2015). All electrodes were $1\frac{3}{16}$ " in diameter to fit inside the cylindrical reactor interior. Fig. 24 is a schematic representation of the reactor used, which depicts the flow-through electrode configuration as well as the dimensions of the system. 200mM NaCl solution entered the anode chamber, passed through the inactive anode electrode, through two CDI electrodes, and exited through the cathode chamber. To speed progress, desalination cycling was done under abiotic conditions with desalination energy provided by a DC power source.

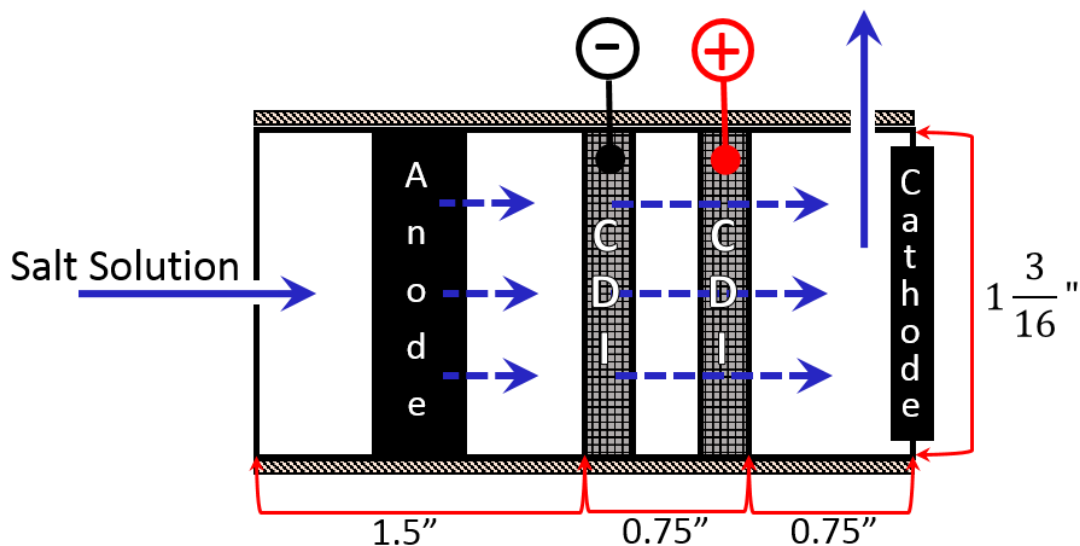


Figure 24: A novel flow-through MCD was for abiotic testing of the CDI using control automation.

Control and data monitoring were performed by two separate systems to minimize electrical interference between relay power and the electrical conductivity circuits. The system was designed to control and monitor up to four MCDs simultaneously and was powered by two Arduino Uno R3 microcontrollers (Arduino, LLC). To switch the system between desalination and regeneration mode, a system state control was designed. Electrical connections to the CDI electrodes were connected to the “common” port of two dual-state relay switches. The “normally open” (NO) ports of the relays were connected to the positive and negative leads from a DC power source while the “normally closed” (NC) ports were connected together. While the relays were powered on, the NO connections were activated and DC power was sent to the CDI electrodes. Otherwise, the NC connections were active and the CDI was short-circuited. To maintain continuous salt concentration at the inlet to the MCD, two salt solution reservoirs were used. Water always pumped out of one reservoir, through the MCD, and into the second reservoir during experimentation. When the effluent reservoir became full, a float switch would signal the Arduino to

swap the influent/effluent reservoirs. Latching solenoids controlled by the Arduino switched the influent/effluent reservoirs quickly to maintain experimental continuity. A timer controlled the system state and any half-cycle time interval for desalination and regeneration could be programmed for.

Electrical conductivity (EC) circuits (EC 3.0, Atlas Scientific, New York) and probes (k1.0, Atlas Scientific, New York) were integrated into a second Arduino for system monitoring. The EC circuits were easily integrated into the custom conductivity, voltage, and current monitoring setup with modification of sample code provided by Atlas Scientific on their website. Voltage was monitored using the analog ports on the Arduino with a reference voltage of 1.1V and 10-bit resolution. Highly precise voltage measurements were not needed since the DC power supply provided sufficient power to maintain constant voltage, which was set at either 1.2, 0.6 or 0.3. In each loop of the monitoring program, conductivity across all connected probes was read first, followed by the voltage across the CDI electrodes. After all data was gathered for the current loop, the data was sent through a USB serial connection to a computer where it was received by a customized version of the program Arduino Excel Commander (www.robertovalgolio.com). The total data storage capacity of this set up was only limited by the maximum spreadsheet size allowed in Microsoft Excel, which is over 1.04 million rows. Data loss was therefore not expected to be an issue. Current across the CDI was also monitored, which was done by a Keithley data acquisition system as described in Chapter 2 because higher precision was needed to read the low current values (less than mA). Fig. 25 below contains a process schematic of the control and monitoring systems, fig. 26 contains a picture of the control system, and fig. 27 contains a picture of the monitoring system.

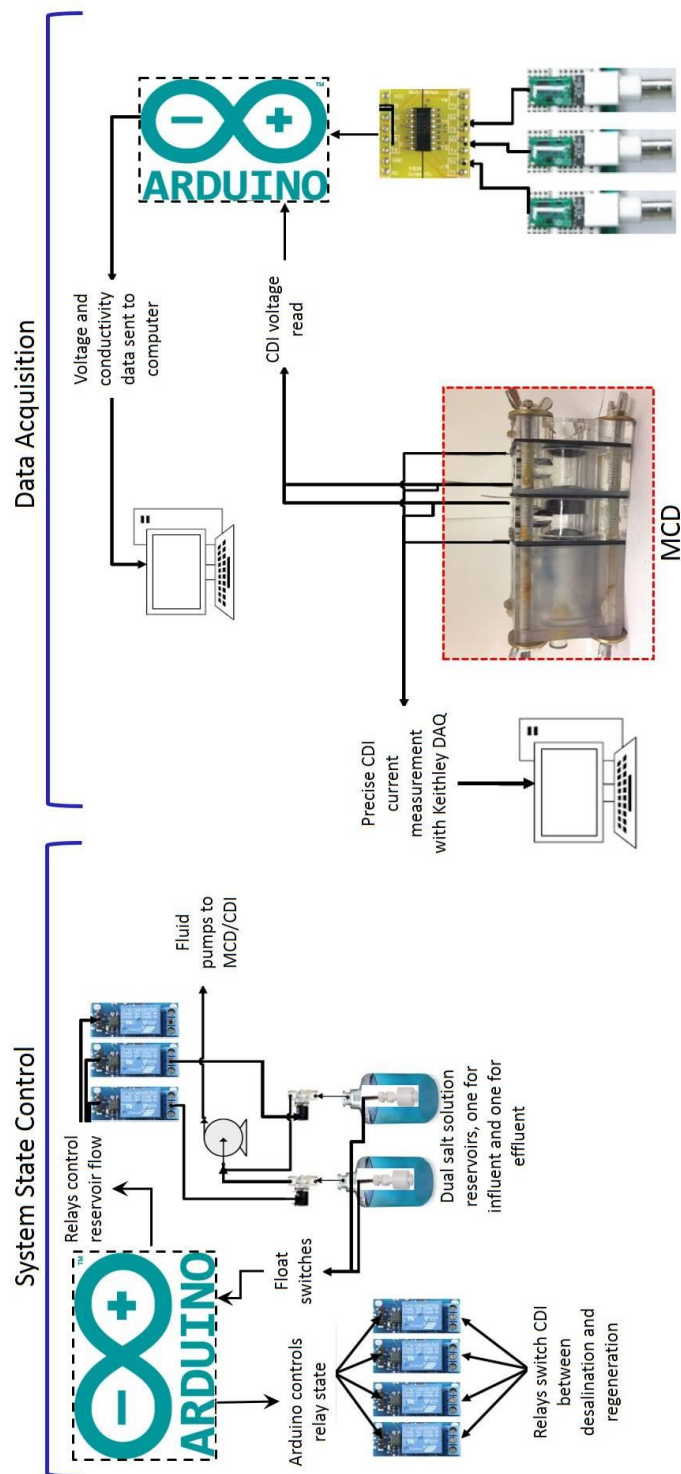


Figure 25: Process diagram for the separated system state controls and data acquisition and monitoring systems. One Arduino Uno R3 was used for each of the two systems, which were powered separately through 9V 1A AC/DC wall adapters.

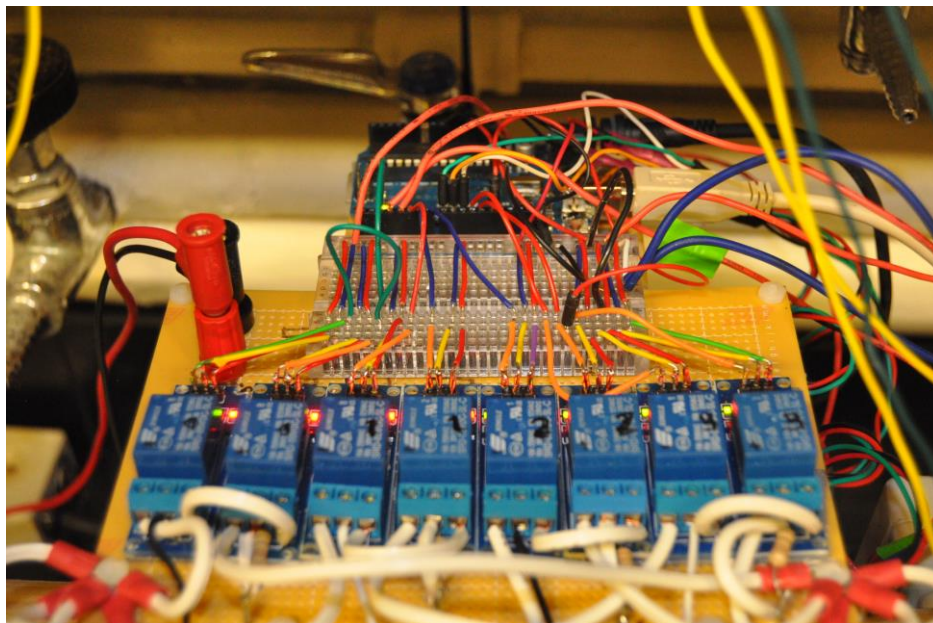


Figure 26: Control was carried out by two relay switches per reactor that were controlled by a standalone Arduino Uno R3.

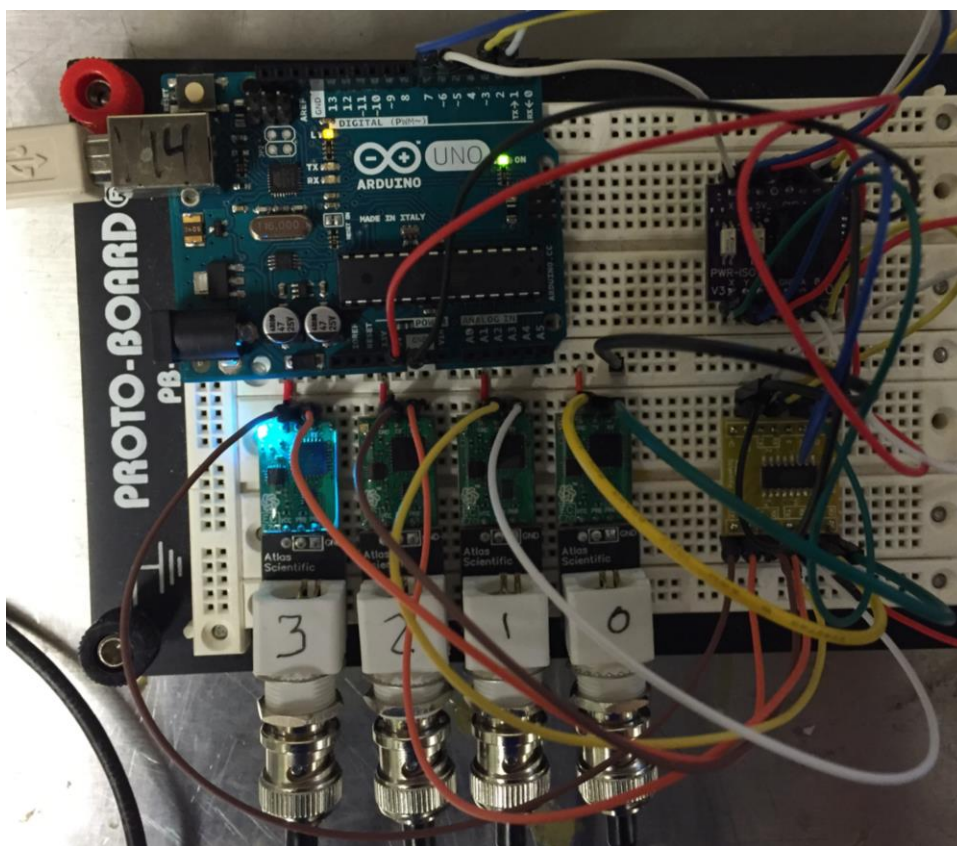


Figure 27: Data acquisition and monitoring was carried out by four EC 3.0 conductivity circuits (Atlas Scientific) connected to an Arduino Uno R3. This system

was connected to a computer serially where data was sent by the Arduino to a MS Excel spreadsheet.

Results and discussion

When a CDI or MCD reactor is first put online chemisorption of salts to the carbon electrodes occurs, a process which is not easily reversed. Therefore, to analyze a CDI system under real-world operational conditions several desalination and regeneration cycles must be performed (Porada et al. 2013). Eventually, a dynamic equilibrium is reached where the desalination performance of the system does not fluctuate substantially over time. The control and monitoring systems developed in this study successfully performed dynamic equilibrium tests for over four months, with the longest continuous data gathering period lasting more than five days. During this time, no human interaction was needed to keep the system going. While the solution reservoir inlets were covered, salt solution loss to evaporation was observed and longer experiments were not performed to maintain stable solution conductivity over time. Raw output data typical of the Arduino monitor are presented in fig. 28.

During desalination, conductivity at the outlet of the reactor is reduced. In regeneration mode, the adsorbed salts are released back into solution and the conductivity at the outlet of the reactor increases. The trend of desalination and regeneration is clear in fig. 28, which is a snapshot of one dynamic equilibrium test. For reporting purposes, the conductivity can be converted into salt concentration if the ions in solution are known. In this experiment NaCl was the only salt used and in the conductivity range used conductivity can be converted to concentration through a linear relationship. Fig. 29 contains similar data to fig. 28 from a different experiment, and is in terms of the concentration difference between the inlet (C_{in}) and the outlet (C_{out}). From this figure it is clear that the system state changes every 20

minutes exactly. With minimal human interaction during the dynamic equilibrium tests, timing errors were eliminated, instantaneous state-switching was achieved, and workers were freed up for more important tasks.

The system presented in this section is proof-of-concept that low cost and low energy consuming microcontrollers can be used monitor and control MCD systems. Large investments are generally needed to develop controls for new water treatment systems, but an interdisciplinary understanding of environmental engineering systems and control design allowed for a completely custom and low-cost automation system to be developed. Without the need for expensive system-specific controls and monitoring devices, the cost of operation of MCD can be greatly reduced both in the laboratory and in the field. Development is ongoing and future plans include using conductivity readings as feedback to determine the system state. There are plans to apply the principles of this system to control a series of larger-scale MCD reactors for studies on a pilot-scale MCD system currently being developed at the University of Colorado.

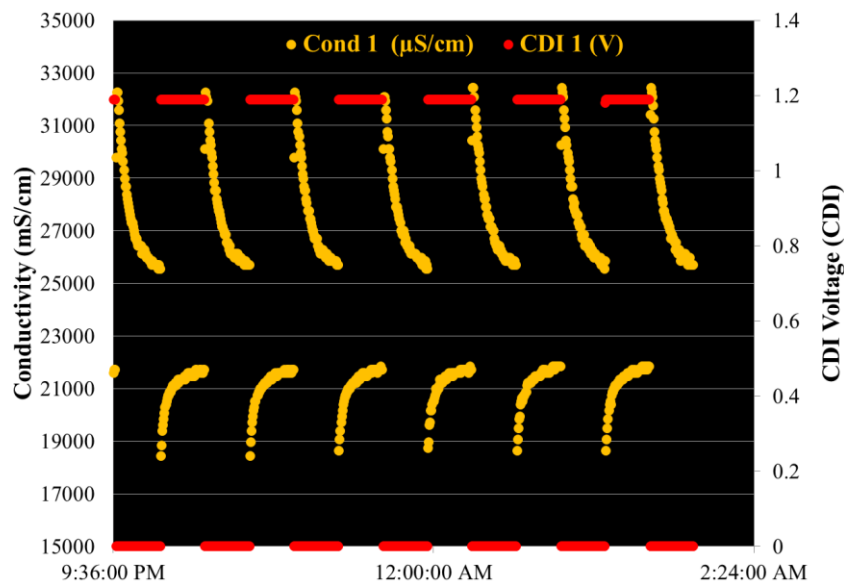


Figure 28: A snapshot of the raw conductivity (yellow) and voltage (red) data output in MS Excel. During voltage application, effluent conductivity drops immediately and eventually rises up to the influent conductivity. Short circuiting to zero volts releases ions back into solution, regenerating the electrodes.

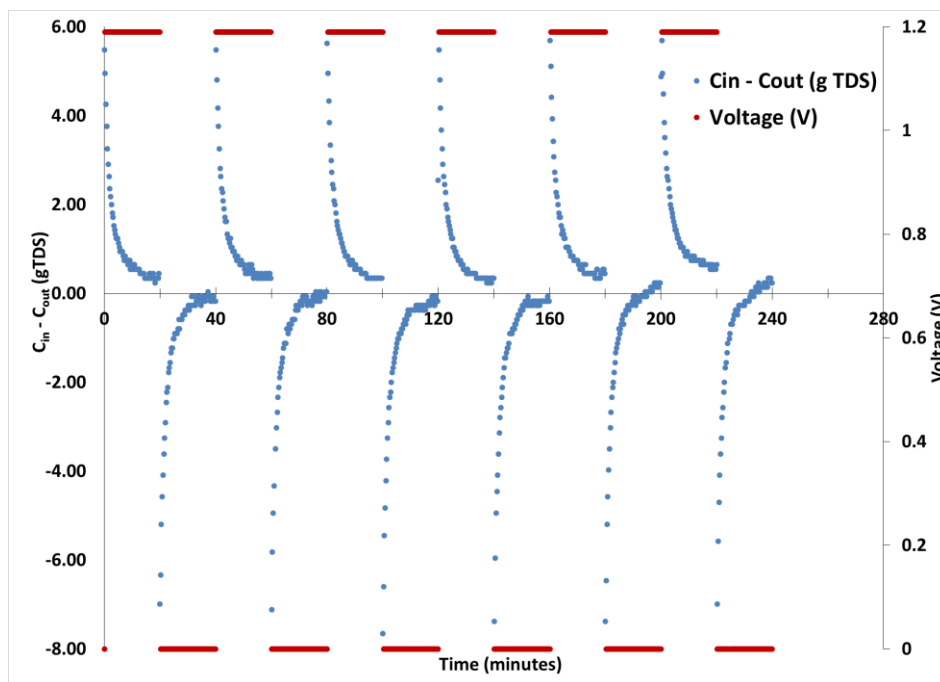


Figure 29: $C_{in} - C_{out}$ data from an experimental run.

Conclusion

While the controls developed in this section were used on abiotic reactors, the system can be easily applied to biotic MCD operation. A third relay switch would be needed per reactor to put a load such as an energy harvester across the MFC portion of the MCD during the regeneration cycle. The monitoring system can be modified to provide feedback to the state controls to automatically switch states based on effluent conductivity for full MCD automation in the field. Feedback interrupt loops may be adopted from the automatic catholyte replacement system described in the previous section to facilitate the state changes. With the focus on field application, modifications can be made for monitoring reservoirs, reactor pressure, flow rate, voltage, and conductivity for performance optimization and implementation of fail-safe response mechanisms. Work on combining the control systems described in this chapter is ongoing and there are plans to integrate the new system into a pilot-scale MCD system.

V. CONCLUSION

This thesis demonstrates the use of interdisciplinary skills for the development of a new bioelectrochemical system design and accompanied control automation systems for wastewater treatment. With the end goal of field application of an innovative produced water treatment system, an incremental approach was taken to the research and development process. First, the spiral wound configuration was investigated and standard manufacturing methods for the systems were developed. With standard procedures for manufacture, consistent and replicable spiral wound microbial fuel cells were built and tested. The spiral wound configuration proved very promising for its low internal ohmic resistance of less than 1Ω , high surface area to volume ratios between $350\text{ m}^2/\text{m}^3$ and $700\text{ m}^2/\text{m}^3$, and power densities of $42\text{ W}/\text{m}^3$ (total anode volume) and $170\text{ W}/\text{m}^3$ (effective anode volume). A tightly wound spiral allowed the high performance, which would have been otherwise impossible without the combined knowledge of manufacturing, adhesives, and microbial fuel cells.

The next step was to apply the new spiral wound configuration to microbial capacitive deionization (MCD). Incremental size increases were made from the 3" long microbial fuel cells alongside manufacturing and design improvements until pilot-scale 40" long MCD reactors were achieved. A machine was built for to house the reactor materials and incrementally turn them into spiral form during adhesive application. Two swMCDs were built and acclimated. However, one reactor failed after acclimation and could not be repaired after irreparable damage was done

removing it from its PVC housing. The functioning reactor experienced short-circuiting between capacitive deionization electrodes as a result of unstable electrode material and insufficient physical separation. However, the reactor still achieved maximum a high power density and current outputs of 89 W/m³ power and 228mA respectively while operating on 100% produced water. Future design improvements should include improved electrode and separator material in the capacitive deionization chamber to prevent short-circuiting, reduce power requirements, and improve desalination performance. Even with the design flaws mentioned, the single reactor removed salts at a rate 10.2 g TDS/L/day, which can be easily improved upon. Ongoing work on this project includes incorporating the design improvements mentioned above to build, test, and implement new spiral wound desalination reactors for energy neutral produced water treatment.

Wastewater treatment systems must be easy to use in the field and generally require a degree of automation. Microbial fuel cell automation was explored for catholyte replacement in the laboratory setting. Voltage output from the system was used as feedback for the control system, which replaced the catholyte automatically to maintain high voltage output. The system developed can be modified to maintain any voltage output desired given a constant influent stream of wastewater. A more complex system was also developed to automate microbial capacitive deionization systems as well. Separate control and monitoring systems allowed for stable conductivity readings and experiment-quality data output. While the system was used exclusively in the laboratory setting, there are plans to adapt it to a new pilot-scale MDC system for field application.

Wastewater treatment is a rapidly evolving field and among new stringent effluent requirements there is a push to move facilities off the electrical grid. Energy requirements for traditional systems are very high and bioelectrochemical

systems are a promising platform technology to harvest the incredible amount of embodied energy in wastewater. Exoelectrogenic bacteria in bioelectrochemical systems produce electricity directly from wastewater without the need for energy conversion machinery. Configuration of the systems is currently a bottleneck to field application, and the new high performance spiral wound reactor configuration developed proved promising for both wastewater treatment and treating oil and gas produced water. With a greater understanding of the manufacture, operation, and control of the complex reactor systems presented here, a future of energy-neutrality in wastewater treatment is one step closer.

REFERENCES

- Aelterman, Peter, Korneel Rabaey, Hai The Pham, Nico Boon, and Willy Verstraete. 2006. "Continuous electricity generation at high voltages and currents using stacked microbial fuel cells." *Environ. Sci. Technol.* no. 40 (10):3388-3394.
- Alleman, J. E., and T. B. S. Prakasam. 1983. "Reflections on seven decades of activated sludge history." *Water pollution control federation* no. 55 (5):436-443.
- Benjamin, Mark M., and Desmond F. Lawler. 2013. *Water quality engineering: Physical and chemical treatment processes*. United States: John Wiley & Sons, Inc.
- Biesheuvel, P. M., and A. van der Wal. 2010. "Membrane capacitive deionization." *Membrane Sci.* no. 346:256-262.
- C.E. Clark, J.A. Veil. 2009. Produced water volumes and management practices in the United States. Environmental Science Division, Argonne National Lab for the U.S. Department of Energy, Office of Fossil Energy, National Energy Technology Laboratory.
- Do-Quang, Z., A. Cockx, A. Liné, and M. Roustan. 1999. "Computational fluid dynamics applied to water and wastewater treatment facility modeling." *Environ. Eng. and Policy* no. 1 (3):137-147.
- Fan, Yanzhen, Sun-kee Han, and Hong Liu. 2012. "Improve performance of CEA microbial fuel cells with increased reactor size." *Energy & Environmental Science* no. 5:8273-8280.
- Forrestal, C., Z. Huang, and Z. Ren. 2014. "Percarbonate as a naturally buffering catholyte for microbial fuel cells." *Biores. Technol.* no. 172:429-432.
- Forrestal, C., Z. Stoll, P. Xu, and Z. Ren. 2015. "Microbial capacitive desalination for integrated organic matter and salt removal and energy production from unconventional natural gas produced water." *Environ. Sci.: Water Res.* no. 47 (1):47-55.
- Forrestal, Casey, Pei Xu, and Zhiyong Ren. 2012. "Sustainable desalination using a microbial capacitive desalination cell." *Energy & Environmental Science* no. 5:7161-7167.
- Haeger, A., C. Forrestal, P. Xu, and Z. J. Ren. 2014. "High performance spiral wound microbial fuel cell with hydraulic characterization." *Biores. Technol.* no. 174:287-293.
- Huggins, T., H. Wang, J. Kearns, P. Jenkins, and Z.J. Ren. 2014. "Biochar as a sustainable electrode material for electricity production in microbial fuel cells." *Bioresour. Technol.* no. 157:114-119.

- Jacobson, K., D. M. Drew, and Z. He. 2011. "Use of a liter-scale microbial desalination cell as a platform to study bioelectrochemical desalination with salt solution or artificial seawater." *Environ. Sci. Technol.* no. 45 (10):4652-4657.
- Jia, Boyang, Dawei Hu, Beizhen Xie, Kun Dong, and Hong Liu. 2013. "Increased power density from a spiral wound microbial fuel cell." *Biosensors and Bioelectronics* no. 41:894-897.
- Keranen, K. M., M. Weingarten, G. A. Abers, and S. Ge. 2014. "Sharp increase in central Oklahoma seismicity since 2008 induced by massive water injection." *Science* no. 345:448-451.
- Lee, J-B., K-K. Park, H-M. Eum, and C-W. Lee. 2006. "Desalination of a thermal power plant wastewater by membrane capacitive deionization." *Desalination* no. 196:125-134.
- Li, W. W., H. Q. Yu, and Z. He. 2014. "Towards sustainable wastewater treatment by using microbial fuel cells-centered technologies." *Energy & Environmental Science* no. 7:911-924.
- Liu, H., and B. Logan. 2004. "Electricity generation using an air-cathode single chamber microbial fuel cell in the presence and absence of a proton exchange membrane." *Environ. Sci. Technol.* no. 38 (14):4040-4046.
- Logan, B. E. 2012. "Essential data and techniques for conducting microbial fuel cell and other types of bioelectrochemical system experiments." *ChemSusChem* no. 5 (6):988-994.
- Logan, Bruce E. , Hamelers Bert, Rene Rozendal, Uwe Schroder, Jurg Keller, Stefano Freguia, Peter Aelterman, Willy Verstraete, and Korneal Rabaey. 2006. Microbial fuel cells: Methodology and technology. *Environmental Science & Technology*.
- Logan, Bruce E., and Korneal Rabaey. 2012. "Conversion of wastes into bioelectricity and chemicals using microbial electrochemical technologies." *Science* no. 337:686-690.
- Lu, Lu, Hadi Yazdi, Song Jin, Paul H. Fallgren, and Zhiyong Jason Ren. 2014. "Enhanced bioremediation of hydrocarbon-contaminated soil using pilot-scale bioelectrochemical systems." *Hazardous Materials* no. 274:8-15.
- Ma, D., C. Forrestal, M. Ji, R. Li, H. Ma, and Z. Ren. 2015. "Membrane configuration influences microbial capacitive desalination performance." *Environ. Sci.: Water Res. Technol.*
- McCarty, P. L., J. Bae, and J. Kim. 2011. "Domestic wastewater treatment as a net energy producer - Can this be achieved?" *Environ. Sci. Technol.* no. 45:7100-7106.
- Oren, Y. 2008. "Capacitive deionization (CDI) for desalination and water treatment - past, present and future (a review)." *Desalination* no. 228:10-29.
- Porada, S., R. Zhao, A. van der Wal, V. Presser, and P. M. Biesheuvel. 2013. "Review on the science and technology of water desalination by capacitive deionization." *Prog. in Mat. Sci.* no. 58 (8):1388-1442.
- Rabaey, Korneel, Peter Clauwaert, Peter Aelterman, and Willy Verstraete. 2005. "Tubular microbial fuel cells for efficient electricity generation." *Environ. Sci. Technol.* no. 39 (20):9077-8082.

- Riley, P. L., C. E. Milstead, A. L. Lloyd, M. W. Seroy, and M. Tagami. 1977. "Spiral-wound thin-film composite membrane systems for brackish and seawater desalination by reverse osmosis." *Desalination* no. 23 (1-3):331-335.
- Savoie, R. 1973. "Latching solenoid valve." *Rev. Sci. Instrum.* no. 44:1432-1433.
- Shizas, I., and D. M. Bagley. 2004. "Experimental determination of energy content of unknown organics in municipal wastewater streams." *J. Energy Engineering* no. 130 (2):45-53.
- Suss, M. E., T. F. Baumann, W. L. Bourcier, C. M. Spadaccini, K. A. Rose, J. G. Santiago, and M. Stadermann. 2012. "Capacitive desalination with flow-through electrodes." *Energy & Environmental Science* no. 5:9511-9519.
- USEPA. 2001. The United States experience with economic incentives for protecting the environment. Office of Policy, Economics, and Innovation.
- USEPA. 2008. Ensuring a sustainable future: An energy management guidebook for wastewater and water facilities.
- USEPA. 2009. Clean energy opportunities in water and wastewater treatment facilities background and resources.
- USEPA. *Class II Wells - Oil and gas related injection wells (class II)*, 5/09/2012 2012. Available from <http://water.epa.gov/type/groundwater/uic/class2/>.
- Wang, Heming, and Z. J. Ren. 2013. "A comprehensive review of microbial electrochemical technology systems as a platform technology." *Biotechnology Advances* no. 31 (8):1796-1807.
- Welgemoed, T. J., and C. F. Schutte. 2005. "Capacitive deionization technology: An alternative desalination solution." *Desalination* no. 183:327-340.
- Xu, Y., X. Peng, C. Y. Tang, Q. S. Fu, and S. Nie. 2010. "Effect of draw solution concentration and operating conditions on forward osmosis and pressure retarded osmosis performance in spiral wound module." *J. Mem. Sci.* no. 348 (1-2):298-309.
- Zhang, X., S. Cheng, X. Wang, X. Huang, and B.E. Logan. 2009. "Separator characteristics for increasing performance of microbial fuel cells." *Environ. Sci. Technol.* no. 43 (21):8456-8461.
- Zhang, X., S. Liang, X. Huang, and B.E. Logan. 2011. "Scalable air cathode microbial fuel cells using glass fiber separators, plastic mesh supporters, and graphite fiber brush anodes." *Bioresour. Technol.* no. 102 (1):372-375.

APPENDIX

A. AUTOMATED CHEMICAL CATHOLYTE FEEDING PROGRAM FOR MICROBIAL FUEL CELLS

/*This program is written in C/C++ and is compiled and uploaded to the Arduino board by the Arduino IDE*/

```
#include <LiquidCrystal.h>
LiquidCrystal lcd(12, 11, 10, 9, 3, 2);

// “va” are valves. There are three valves in this case connected to relays which power
the opening and closing of the valves
// “po” are the relays used to power the solenoids
int po1 = 4;
int va1 = 5;
int va2 = 6;
int po2 = 7;
int va3 = 8;
int button = 13; //Begin and manual flush button
int f0 = 14; //floats on Analog pins 0 & 1 & 2
int f1 = 15;
int f2 = 16;

// Variables
float vSense;
float volt = 0; // Current voltage read
float lastV = 0; // Last voltage read
float deltaV = 0; // Difference between current and previous voltage reads
int y; //Counter
int z = 0; //Counter
int flag = 0; //Flag that informs whether or not catholyte replacement is needed

void setup() {
  analogReference(INTERNAL);
```

```

pinMode(f0, INPUT); pinMode(f1, INPUT); pinMode(f2, INPUT); pinMode(button,
INPUT); pinMode(A6, INPUT); pinMode(po1, OUTPUT); pinMode(po2, OUTPUT);
pinMode(va1, OUTPUT); pinMode(va2, OUTPUT); pinMode(va3, OUTPUT);
  lcd.begin(16,2); lcd.print(" The AutoMFC");
  lcd.setCursor(0, 1); lcd.print("Haeger CUBoulder");
  delay(3000);
lcd.clear();

// Prompt user to make sure reservoir is full before beginning
lcd.clear(); lcd.print("Fill Reservoir"); lcd.setCursor(0, 1); lcd.print("And Press
Button");
while (digitalRead(button) == LOW) {delay(10);}
}

void loop() {
// Initialize system by setting all valves and polarization relays to LOW
digitalWrite(po1, LOW); digitalWrite(po2, LOW); digitalWrite(va1, LOW);
digitalWrite(va2, LOW); digitalWrite(va3, LOW);

// Begin the replenishment cycle by checking reservoir for sufficient volume
lcd.clear(); y = 0;
while (digitalRead(f0) == LOW) {
  lcd.clear(); lcd.print("Tank is empty"); lcd.setCursor(0, 1); lcd.print("Time= ");
lcd.setCursor(7, 1); lcd.print(y, 4); lcd.setCursor(10, 1); lcd.print("sec"); delay(1000);}
  lcd.clear(); lcd.print("Draining Cathode"); lcd.setCursor(0, 1); lcd.print("Please
Wait");

// Drain cathode by double opening the drain valve - va3, then double close
digitalWrite(va3, HIGH); delay(50); digitalWrite(va3, LOW); delay(50);
digitalWrite(va3, HIGH); delay(50); digitalWrite(va3, LOW);
delay(100000);
digitalWrite(po1, HIGH); digitalWrite(po2, HIGH); delay(10);
digitalWrite(va3, HIGH); delay(50); digitalWrite(va3, LOW); delay(50);
digitalWrite(va3, HIGH); delay(50); digitalWrite(va3, LOW); delay(50);
digitalWrite(po1, LOW); digitalWrite(po2, LOW); delay(10);

// Fill cathode 1 first
lcd.clear(); lcd.print("CATHODE1 FILLING"); lcd.setCursor(0, 1); lcd.print("PLEASE
WAIT");
digitalWrite(va1, HIGH); delay(50); digitalWrite(va1, LOW); delay(50);
digitalWrite(va1, HIGH); delay(50); digitalWrite(va1, LOW); delay(10);
while (digitalRead(f1) == HIGH) {delay(10);}
digitalWrite(po1, HIGH); digitalWrite(po2, HIGH); delay(10);

```

```

digitalWrite(va1, HIGH); delay(50); digitalWrite(va1, LOW); delay(50);
digitalWrite(va1, HIGH); delay(50); digitalWrite(va1, LOW); delay(50);
digitalWrite(po1, LOW); digitalWrite(po2, LOW); delay(10);
// Fill cathode 2 next
lcd.clear(); lcd.print("CATHODE2 FILLING"); lcd.setCursor(0, 1); lcd.print("PLEASE
WAIT");
digitalWrite(va2, HIGH); delay(50); digitalWrite(va2, LOW); delay(50);
digitalWrite(va2, HIGH); delay(50); digitalWrite(va2, LOW); delay(10);
while (digitalRead(f2) == HIGH) {delay(10);}
digitalWrite(po1, HIGH); digitalWrite(po2, HIGH); delay(10);
digitalWrite(va2, HIGH); delay(50); digitalWrite(va2, LOW); delay(50);
digitalWrite(va2, HIGH); delay(50); digitalWrite(va2, LOW); delay(50);
digitalWrite(po1, LOW); digitalWrite(po2, LOW); delay(10);

lcd.clear(); lcd.print("FILL COMPLETE"); lcd.setCursor(0, 1); lcd.print("TIME FOR
A NAP");
delay(3000); lcd.clear(); lcd.print("AutoMFC Working."); delay(3000);

// This section of the program records change in voltage between each 5 minute time
step. If two consecutive voltage reads indicate decreasing voltage,
// the program exits the loop and begins the flushing cycle at the top of the program.

// Reset flag and voltage values
flag = 0;
volt = 0;
lastV = 0;
deltaV = 0;

// Stay in this loop until voltage on one of the reactors begins to drop. deltaV is the
change in voltage from the previous time step and (volt-lastV) is the voltage change
in the current time step
// If voltage is constant or increasing the catholyte is assumed to be performing well.
When voltage decreases by 0.1 mV or more for two consecutive time-steps the
catholyte is replaced automatically.
// A button was installed to initiate replacement of the catholyte manually.
// After the flag is set voltage and voltage change is printed to the LCD screen.

while ((flag == 0) && (digitalRead(button) == LOW)) {
  volt = analogRead(A5) * (1.100 / 1023.000);
  if ((deltaV < 0) && ((volt - lastV) < 0)) { flag = 1; }
  else { flag = 0; }

  deltaV = volt - lastV;
  lcd.clear();

```

```
    lcd.print("V="); lcd.setCursor(3, 0); lcd.print(volt, 5); lcd.setCursor(10, 0); lcd.print("
Volts");
    lcd.setCursor(0,1); lcd.print("dV="); lcd.setCursor(4, 1); lcd.print(deltaV, 5);
    lcd.setCursor(14, 1); lcd.print(y, 2);
    lastV = volt;

// 6 minute delay with button interupt between main loop cycles
    z = 0;
    while((z < 360) && (digitalRead(button) == LOW)){
        delay(1000); z++; }
    }
    y++;
}
```

B. AUTOMATED CONDUCTIVITY AND VOLTAGE MONITORING PROGRAM FOR MCD AND CDI

```

/*
This program is written in C/C++ and is compiled and uploaded to the Arduino board
by the Arduino IDE

Portions of this code were adapted from sample code provided for EC circuits at
www.atlas-scientific.com
*/

#include <SoftwareSerial.h> //SoftSerial emulates serial ports on digital I/O pins
#define rx 2 //define rx pin
#define tx 3 //define tx pin

SoftwareSerial myserial(rx, tx); //define how the soft serial port is going to work.

char EC_data[48]; //20 byte character array to hold incoming data from the
EC.
char computerdata[20]; //20 byte character array to hold incoming data from
a pc/mac/other.
byte received_from_computer=0; //Holds number of characters received from comp
byte received_from_sensor=0; //Holds number of characters received from sens
byte string_received=0; //used to identify when string is received from EC
circuit

float EC_float=0; //EC value

char *EC; //char pointer used in string parsing

//Variables to control the serial connector
int s0 = 6; //Arduino pin 6 to control pin S0
int s1 = 7; //Arduino pin 7 to control pin S1

int r=0; // Starting index for Excel logging
int i,x,p=0;
int z=1;
float volts,sum,voltage0,voltage1,voltage2;

//Strings to output EC values for channels 0-2
String EC0;

```

```

String EC1;
String EC2;

char voltage[2];

void setup(){
//Serial and Softserial baud = 38400
  Serial.begin(38400); myserial.begin(38400);

//These are the selector outputs to decide which channels are being used on the 4 port
serial connector
  pinMode(s1, OUTPUT); pinMode(s0, OUTPUT);

//Analog input channels used to read voltage
  pinMode(A0,INPUT); pinMode(A1,INPUT); pinMode(A2,INPUT);

/* EC circuits sometimes need to receive a command upon startup before further
commands can be received.
  Here the circuits are asked to read conductivity once each before the experiment
begins.      */

digitalWrite(s0, LOW); digitalWrite(s1, LOW); //Ch. 0
  delay(1000); myserial.print("r");myserial.print("\r"); delay(2000);
digitalWrite(s0, HIGH); digitalWrite(s1, LOW); //Ch. 1
  delay(1000); myserial.print("r");myserial.print("\r"); delay(2000);
digitalWrite(s0, LOW); digitalWrite(s1, HIGH); //Ch. 2
  delay(1000); myserial.print("r");myserial.print("\r"); delay(2000);
}

void loop(){          //Begin main loop
delay(5000);

//First, the "r" read command is sent to the EC circuit to wake it up. No data is
collected here.
// Next, the "r" read command is sent to the EC circuit and a response is listened for.
// Data is stored in either EC0, EC1, EC2, or EC3 variables

/***** Channel 0 *****/
digitalWrite(s0, LOW); digitalWrite(s1, LOW);

delay(500);

myserial.print("r");myserial.print("\r");

```

```

while(1){
  myserial.print("r"); myserial.print("\r");
  if(myserial.available() > 0){ //if we see that the EC Circuit has sent a character.
    received_from_sensor=myserial.readBytesUntil(13,EC_data,48); //we read the
    data sent from EC Circuit until we see a <CR>. We also count how many character
    have been received.
    EC_data[received_from_sensor]=0; //we add a 0 to the spot in the array just after
    the last character we received. This will stop us from transmitting incorrect data that
    may have been left in the buffer.

    if((EC_data[0] >= 48) && (EC_data[0] <=57)){ //if ec_data[0] is a digit and not a
    letter
      pars_data(); EC0=EC; break;
    }
    else
      EC1="A";
      break;
    }
  }
}

EC=0; EC_data[0]=(char)0;

delay(5000);

/***** Channel 1 *****/
digitalWrite(s0, HIGH); digitalWrite(s1, LOW);

delay(500);

myserial.print("r");myserial.print("\r");

while(1){
  myserial.print("r"); myserial.print("\r");
  if(myserial.available() > 0){ //if we see that the EC Circuit has sent a character.
    received_from_sensor=myserial.readBytesUntil(13,EC_data,48); //we read the
    data sent from EC Circuit until we see a <CR>. We also count how many character
    have been received.
    EC_data[received_from_sensor]=0; //we add a 0 to the spot in the array just after
    the last character we received. This will stop us from transmitting incorrect data that
    may have been left in the buffer.

    if((EC_data[0] >= 48) && (EC_data[0] <=57)){ //if ec_data[0] is a digit and not a
    letter
      pars_data(); EC1=EC; break;

```

```

    }
    else
        EC1="A";
        break;
    }
}

EC=0; EC_data[0]=(char)0;

delay(5000);

/***** Channel 2 *****/
digitalWrite(s0, LOW); digitalWrite(s1, HIGH);

delay(500);

myserial.print("r");myserial.print("\r");

while(1){
    myserial.print("r"); myserial.print("\r");
    if(myserial.available() > 0){ //if we see that the EC Circuit has sent a character.
        received_from_sensor=myserial.readBytesUntil(13,EC_data,48); //we read the
        data sent from EC Circuit until we see a <CR>. We also count how many character
        have been received.
        EC_data[received_from_sensor]=0; //we add a 0 to the spot in the array just after
        the last character we received. This will stop us from transmitting incorrect data that
        may have been left in the buffer.

        if((EC_data[0] >= 48) && (EC_data[0] <=57)){ //if ec_data[0] is a digit and not a
        letter
            pars_data(); EC2=EC; break;
        }
        else
            EC2="A";
            break;
        }
    }

EC=0; EC_data[0]=(char)0;

//delay(5000);

//Read voltages
volts=analogRead(A0);

```



```
voltage0 = volts * 5.00/1023;
delay(100);
volts=analogRead(A1);
voltage1 = volts * 5.00/1023;
delay(100);
volts=analogRead(A2);
voltage2 = volts * 5.00/1023;

/***** Transmit data to Excel *****/
delay(2000);
Serial.print(F("XLS,ARR1,"));
Serial.print(r);
Serial.print(",");
Serial.print("voltage0");
Serial.print(F("\n"));
delay(500);
Serial.print(F("XLS,ARR2,"));
Serial.print(r);
Serial.print(F(","));
Serial.print(EC0);
Serial.print(F("\n"));
delay(500);
Serial.print(F("XLS,ARR3,"));
Serial.print(r);
Serial.print(F(","));
Serial.print("voltage1");
Serial.print(F("\n"));
delay(500);
Serial.print(F("XLS,ARR4,"));
Serial.print(r);
Serial.print(F(","));
Serial.print(EC1);
Serial.print(F("\n"));
delay(500);
Serial.print(F("XLS,ARR5,"));
Serial.print(r);
Serial.print(",");
Serial.print("voltage2");
Serial.print(F("\n"));
delay(500);
Serial.print(F("XLS,ARR6,"));
Serial.print(r);
Serial.print(F(","));
```

```

Serial.print(EC2);
Serial.print(F("\n"));
/*delay(500);
Serial.print(F("XLS,ARR7,"));
Serial.print(r);
Serial.print(F(","));
Serial.print("-");
Serial.print(F("\n"));
delay(500);
Serial.print(F("XLS,ARR8,"));
Serial.print(r);
Serial.print(F(","));
Serial.print("-");
Serial.print(F("\n"));*/
r++; //r corresponds to which row the data is sent to in Excel.
EC0="0";
EC1="0";
EC2="0";
delay(5000);
} //End main loop

//Take only EC data from string returned from EC Circuit
void pars_data(){
    EC=strtok(EC_data, ",");
}

```

C. SYSTEM STATE CONTROL PROGRAM FOR CDI AND MCD

```
/*
```

This is the System State Control program for MCD and CDI reactors. The program switches the systems between desalination and regeneration based on a stand-alone timer that is not interrupted by any feedback. Meanwhile, two reservoirs are monitored by float switches so that the full reservoir is emptied completely before the second reservoir is drawn from. One reservoir is drawn from while the second is being filled with reactor effluent at all times. Switching occurs within milliseconds.

This program is written in C/C++ and is compiled and uploaded to the Arduino board by the Arduino IDE

```
*/
```

```
// set timing variables
```

```
unsigned long time = 0;
```

```
unsigned long oldTime = 0;
```

```
unsigned long dif = 0;
```

```
unsigned long halfCycle = 300000; //5 minutes
```

```
// pwrState=1 for short circuit, pwrState=0 for power on
```

```
int pwrState = 0;
```

```
int floatState = 0;
```

```
// Variables to hold information about the state of the float switches in either reservoir
```

```
int Res2;
```

```
int Res3;
```

```
// Float switches are read on these digital pins
```

```
int float2 = 2;
```

```
int float3 = 3;
```

```
void setup(){
```

```
//Initiate float switches
```

```
pinMode(float2,INPUT);
```

```
pinMode(float3,INPUT);
```

```
//Initiate pins that control relays that power the solenoids
```

```
pinMode(11,OUTPUT);
```

```
pinMode(12,OUTPUT);
```

```
pinMode(13,OUTPUT);
```

```

// Initiate pins used for the relays that control system state
pinMode(0,OUTPUT);
pinMode(1,OUTPUT);
pinMode(4,OUTPUT);
pinMode(5,OUTPUT);
pinMode(6,OUTPUT);
pinMode(7,OUTPUT);
pinMode(8,OUTPUT);
pinMode(9,OUTPUT);

// Begin with power off
pwrOff();

}

void loop(){ //Begin main loop

time = millis(); // Record time
dif = time - oldTime; //Calculate time since last state switch

if (dif > halfCycle){ //Determines if the half-cycle has ended, if so the current power
state is determined and switched to the opposite

if (pwrState == 0){ //POWER OFF
pwrOn(); pwrState = 1;
oldTime = time; dif = 0;}

else if (pwrState == 1){ //POWER ON
pwrOff(); pwrState = 0;
oldTime = time; dif = 0;}

}

// Read the float switches
Res2 = digitalRead(float2);
Res3 = digitalRead(float3);

// This section determines whether the reservoirs are full or not
// When one is full, the switches fire and feed is drawn from the full carboy
// and effluent discharges into the empty carboy

if (floatState == 0 && Res2 == 1){

```

```
digitalWrite(11,LOW); delay(100); digitalWrite(13,LOW); delay(100);
digitalWrite(11,LOW); delay(100); digitalWrite(13,LOW); delay(500);
digitalWrite(12,HIGH); delay(100); digitalWrite(12,LOW); delay(100);
digitalWrite(12,HIGH); delay(100); digitalWrite(12,LOW);
floatState=1;
}
else if (floatState == 1 && Res3 == 1){
digitalWrite(11,HIGH); delay(100); digitalWrite(13,HIGH); delay(100);
digitalWrite(11,HIGH); delay(100); digitalWrite(13,HIGH); delay(100);
digitalWrite(12,HIGH); delay(100); digitalWrite(12,LOW); delay(100);
digitalWrite(12,HIGH); delay(100); digitalWrite(12,LOW); delay(100);
digitalWrite(11,LOW); delay(100); digitalWrite(13,LOW); delay(100);
floatState=0; }
}

void pwrOff(void){
digitalWrite(0,HIGH); digitalWrite(1,HIGH);
digitalWrite(4,HIGH); digitalWrite(5,HIGH);
digitalWrite(6,HIGH); digitalWrite(7,HIGH);
digitalWrite(8,HIGH); digitalWrite(9,HIGH);
digitalWrite(10,LOW);
}

void pwrOn(void){
digitalWrite(0,LOW); digitalWrite(1,LOW);
digitalWrite(4,LOW); digitalWrite(5,LOW);
digitalWrite(6,LOW); digitalWrite(7,LOW);
digitalWrite(8,LOW); digitalWrite(9,LOW);
digitalWrite(10,HIGH);
}
```